Icarus **159**, 468–499 (2002)
doi:10.1006/icar.2002.6902

Small Main-Belt Asteroid Spectroscopic Survey in the Near-Infrared

Thomas H. Burbine[1]

Department of Mineral Sciences, National Museum of Natural History, Smithsonian Institution, Washington, DC 20560-0119
E-mail: burbine.tom@nmnh.si.edu

and

Richard P. Binzel[1]

Department of Earth, Atmospheric, and Planetary Sciences, Massachusetts Institute of Technology, Cambridge, Massachusetts 02139

Received December 4, 2001; revised April 30, 2002

Near-infrared spectra (∼0.90 to ∼1.65 μm) are presented for 181 main-belt asteroids, more than half having diameters less than 20 km. These spectra were measured using a specialized grism at the NASA Infrared Telescope Facility, where the near-infrared wavelength coverage is designed to complement visible wavelength CCD measurements for enhanced mineralogic interpretation. We have focused our analysis on asteroids that appear to have surfaces dominated by olivine or pyroxene since these objects can be best characterized with spectral coverage only out to 1.65 μm. Olivine-dominated A-type asteroids have distinctly redder slopes than olivine found in meteorites, possibly due to surface alteration effects such as micro-meteoroid bombardment simulated by laser irradiation laboratory experiments. K-type asteroids observed within the Eos family tend to be well matched by laboratory spectra of CO3 chondrites, while those independent of the Eos family have a variety of spectral properties. The revealed structure of the 1-μm band for 3628 Božněmcová appears to refute its previously proposed match to ordinary chondrite meteorites. Božněmcová displays a 1-μm band that is unlike that for any currently measured meteorite; however, spectra out to 2.5 μm are needed to conclusively argue that Božněmcová has a surface mineralogy different from that of ordinary chondrites. Extending the spectral coverage of Vestoids out to ∼1.65 μm continues to be consistent with the "genetic" relationship of almost all observed Vestoids with Vesta and the howardites, eucrites, and diogenites. Eucrites/howardites provide the best spectral matches to the observed Vestoids.

Key Words: **asteroids; composition.**

INTRODUCTION

Over 2000 asteroids have been characterized by broadband colors (e.g., Zellner *et al.* 1985) or charge-coupled device (CCD) spectra (e.g., Xu *et al.* 1995) in the visible wavelength region (∼0.4 to ∼1 μm). The most notable of these data sets is the second part of the Small Main-Belt Asteroid Spectroscopic Survey (SMASS II) (Bus and Binzel 2002a), which observed over 1300 main-belt objects with estimated diameters as small as a few kilometers.

It is difficult to determine the mineralogy of an object just using spectral data shortward of 1 μm since many common meteoritic minerals (e.g., olivine, pyroxene) have absorption features that extend past 1 μm. However, only ∼200 asteroids (e.g., Bell *et al*. 1988, Clark *et al.* 1995) have been spectrally characterized past 1 μm. The low number of objects that have been observed in this wavelength region is due primarily to the fact that very few observatories, such as the NASA Infrared Telescope Facility (IRTF) on Mauna Kea, are at altitudes high enough for these observations.

The most widely used near-infrared data set is the 52-color survey (Bell *et al*. 1988), which observed over 100 objects in 52-channels from 0.8 to 2.5 μm. The 52-color survey focused on S asteroids, which later allowed Gaffey *et al.* (1993) to divide the S class into a number of subclasses with interpreted surface compositions that varied from olivine-dominated to olivine/pyroxene mixtures to pyroxene-dominated. The mineralogical characterization of these objects was made using the band center of the 1-μm feature and the ratio of the areas of the 1- and 2-μm features. All of the main-belt 52-color objects had estimated diameters greater than 20 km.

To better characterize the mineralogies of asteroids, the Small Main-Belt Asteroid Spectroscopic Survey in the near-infrared (SMASSIR) was initiated at the IRTF. This survey was begun a few years before the advent of SpeX, the near-infrared spectrograph currently used at the IRTF. Only the spectra of main-belt asteroids will be discussed in this paper. SMASSIR results for many near-Earth objects are discussed in Binzel *et al.* (2001a). SMASSIR has a wavelength coverage from ∼0.9 to ∼1.65 μm and focuses on asteroids thought to have "interesting" surface

[1] Visiting astronomer at the Infrared Telescope Facility, which is operated by the University of Hawaii under contract to the National Aeronautics and Space Administration.

0019-1035/02 $35.00

compositions based on their visible spectra. These objects included olivine-dominated asteroids, objects with V (or J) designations, and proposed meteoritic spectral analogs.

Compared to the 52-color survey, the advantage of SMASSIR is that much fainter main-belt objects (with estimated diameters as small as a few kilometers) can be observed. The disadvantage of SMASSIR is that reflectance data can only be obtained out to $\sim$1.65 μm, allowing only part of the 2-μm feature due to pyroxene to be characterized. The SMASSIR spectral wavelength coverage allows full characterization of the 1-μm feature of olivine and pyroxene. However, the quantitative mineralogical determination of the relative abundances of pyroxene and olivine (Cloutis *et al.* 1986) and the composition of the pyroxene (Adams 1974) requires full measurement of the 2-μm feature.

OBSERVATIONS

SMASSIR data were taken at the Infrared Telescope Facility, which is located at Mauna Kea on the island of Hawaii. A low-resolution "asteroid" grism with appropriate blocking filters designed by Richard Binzel (Binzel *et al.* 2001a) was used to record a simultaneous first-order spectrum from $\sim$0.90 to $\sim$1.65 μm on the National Science Foundation Camera InSb array. The average dispersion is $\sim$0.013 μm per pixel (130 Å per pixel) for an average resolution of $\sim$0.026 μm (2 pixels). The nonlinear wavelength calibration was obtained by taking spectral images of the illuminated dome through a number of narrowband filters having known central wavelengths. In February 1999, some of the calibration filters were removed from the filter wheel. The pixel locations for the remaining filters remained unchanged (to within 1 pixel), giving good confidence that the wavelength calibration error did not exceed 0.02 μm. The SMASSIR wavelengths overlap the visible CCD coverage of SMASS. Spectral coverage past $\sim$1.65 μm is not possible due to the overlap of the second-order spectrum.

Observational parameters for the SMASSIR observations of the objects presented in this paper are given in Appendix A. Burbine (2000) reduced the data taken from January 1997 to May 1999, while data taken from June 1999 to May 2000 were reduced by an undergraduate student (April Deet) under the supervision of Binzel. In the reduction, each asteroid spectrum was divided by a standard (solar analog) star observed at a similar airmass and time to produce the reflectance spectrum for each asteroid relative to the Sun. A number of 52-color objects (e.g., 221 Eos, 349 Dembowska) with well-determined spectral characteristics were observed each night and reduced with a variety of standard stars to check to see if there were any observational problems with any of the standard stars. Each asteroid spectrum was taken in a similar fashion except for 4 Vesta. Due to Vesta's brightness, its spectrum was taken from a defocused image and divided by the spectrum of a defocused standard star.

Multiple images were taken for each asteroid and standard star. Images were obtained in pairs (images "A" and "B") with the spectra falling on alternating parts of the InSb array. As much as possible, the "A" image was repeatedly placed on the same column (and similarly for the "B" image). Image "A" was subtracted by "B" and vice versa to remove background counts from the sky in each image. Spectral data reduction was performed using the Image Reduction and Analysis Facility (IRAF), developed by the National Optical Astronomical Observatories. The IRAF package *apall* was used to produce a spectrum from each image by summing the pixel values within a specified aperture at each point along the dispersion axis and subtracting any remaining background level measured by a fit of the background residing outside the aperture.

Since the different parts of the InSb array may have different sensitivities, spectra from each image from the "A" side of the chip were averaged to produce a composite "A" spectrum for a particular object, and similarly for the "B" side spectra. The composite asteroid spectrum from the "A" side was divided by the spectrum of the composite standard star from the "A" side, and similarly for the "B" side spectra. A requirement for "acceptable" data was good agreement (within the signal-to-noise uncertainties) between the features of "A" and "B" spectra. Mismatching "A" and "B" spectra that could not be reconciled were mutually eliminated from further reduction and analysis (a rare occurrence, happening in about 1% of all cases). As a final step, the mutually consistent "A" and "B" reflectance spectra were averaged to produce the final reflectance spectrum for a particular night. An atmospheric water band centered at $\sim$1.4 μm causes the points between 1.35 and 1.5 μm to be very suspect and not usable for most asteroids due to the large amount of scatter among the points. Due to the problems in correcting for atmospheric water, no corrections have been made and points that appear to have been affected significantly have been deleted. Weaker atmospheric effects are also sometimes present in the spectra at $\sim$0.94 and $\sim$1.15 μm.

To determine possible uncertainties in spectral slope for the asteroids due to airmass differences and other problems due to the atmosphere, we divided each standard star by another standard star (taken on the same evening) observed at a lower airmass. This division produced a "reflectance" spectrum for the higher airmass standard star. A difference in slope (from $\sim$0.92 to $\sim$1.65 μm) of 0% from unity indicates that two standard stars have the same spectral slope. After the division, the average offset in slope from unity was approximately 5% ($4.9 \pm 4.4\%$). This average uncertainty ($\sim$5%) in the spectral slope for an asteroid spectrum at the SMASSIR wavelengths is comparable to slope uncertainties in the visible (Bus 1999).

Error bars were calculated in slightly different ways by Burbine (2000) and in the June 1999–May 2000 data reduced subsequently. Burbine (2000) used Poisson statistics. The signal-to-noise ratio for each image was calculated by dividing the signal (the summed pixel values with the remaining background level removed from the subtracted images) by the noise (the square root of the summed pixel values with no remaining background level removed from the unsubtracted images). The

inverse of the signal-to-noise is the fractional error. The fractional errors for each standard star and asteroid image could be propagated to produce the 1-σ error bars for the final composite spectra. For the latter data, Poisson statistics were also used, but the point-to-point scatter in the final data points was also examined. The final error bar values tabulated correspond to the larger of these values.

Each SMASSIR spectrum was normalized to a visible spectrum. The normalization to the visible spectrum was conducted by first fitting the SMASSIR spectrum with errors using a cubic spline program (Reinsch 1967) that was adapted by Schleicher (personal communication 1993) and has been previously used by Bus (1999). Points that appeared significantly affected by atmospheric water features were not used. The SMASSIR spectra were fit from 0.92 to 1.65 μm at 0.01-μm intervals. The 0.92-μm endpoint was chosen since the SMASS II spectra were fit from 0.44 to 0.92 μm (Bus 1999) and the two fits could be directly overlapped. Also, the number of counts measured shortward of 0.92 μm in SMASSIR is rapidly decreasing, which increases the uncertainty in the value of those points. When SMASSII data were not available, SMASS I and ECAS data were also fit from 0.44 to 0.92 μm. The SMASSIR fit was then normalized to the fitted visible spectrum. The actual SMASSIR spectrum was multiplied by this normalization factor and then overlaid on the visible spectrum to get the best continuous spectrum from $\sim$0.44 to $\sim$1.65 μm.

To determine 1-μm band centers, the cubic spline program was used to fit the overlapping visible and near-infrared spectra over the 1-μm band region. A linear continuum was then divided out of the fitted spectrum so the band minimum would be the band center.

DATA

Appendix A gives the classifications and observing parameters of the SMASSIR objects and Appendix B presents the spectra. For objects observed multiple times, only the observing parameters for the best-quality spectrum are given and plotted. All data are available for downloading at the SMASS Web site (http://smass.mit.edu).

All taxonomic classes mentioned in this paper are from analyses of an asteroid's visible spectrum and are not based on analyses of its near-infrared spectrum. In Appendix A, the classifications given are primarily those of Bus and Binzel (2002b). Using the Tholen taxonomy as its foundation, the Bus and Binzel (2002b) taxonomy contains 26 classes that are defined solely by the presence, absence, shape, and depth of spectral absorption features found in the Bus and Binzel (2002a) CCD spectra. The taxonomy was defined using a combination of analytical techniques as well as human judgment (through visual inspection of the data). A listing of each of the Bus and Binzel (2002b) classes and their spectral characteristics are given in Table I.

TABLE I
Table and Spectral Characteristics of the Bus and Binzel (2002b) Taxonomic Classes

Class	Spectral characteristics
A	Very steep red slope shortward of 0.75 μm and a moderately deep absorption longward of 0.75 μm
B	Linear, featureless spectrum over interval of 0.44–0.92 μm, with negative (bluish) to flat slope
C	Weak to medium UV absorption shortward of 0.55 μm, flat to slightly reddish longward of 0.55 μm
Cb	Linear, featureless spectrum over interval of 0.44–0.92 μm with a flat to slightly reddish spectral slope
Cg	Strong UV feature shortward of 0.55 μm and flat to slightly reddish slope longward of 0.55 μm
Ch	Similar to C type, except for addition of broad, relatively shallow absorption centered near 0.7 μm
Cgh	Similar to Cg spectrum, except for addition of broad, shallow absorption band centered near 0.7 μm
D	Relatively featureless spectrum with a very steep red slope
K	Moderately steep red slope shortward of 0.75 μm, a flat to slightly negative slope longward of 0.75 μm
L	Very steep red slope shortward of 0.75 μm and then becoming approximately flat
Ld	Very steep red slope shortward of 0.7 μm, becoming essentially flat longward of 0.75 μm
O	Red slope from 0.44 to 0.54 μm, less steep from 0.54 to 0.7 μm, deep absorption longward of 0.75 μm
Q	Moderately steep red slope shortward of 0.7 μm and deep, rounded absorption longward of 0.75 μm
R	Very steep red slope shortward of 0.7 μm, and a deep absorption longward of 0.75 μm
S	Steep, reddish slope shortward of 0.7 μm and a moderate to deep absorption longward of 0.75 μm
Sa	Spectrum intermediate between S and A types
Sk	Spectrum intermediate between S and K types
Sl	Spectrum intermediate between S and L types
Sq	Spectrum intermediate between S and Q types
Sr	Spectrum intermediate between S and R types
T	Moderately steep red slope shortward of 0.75 μm, becoming flat longward of 0.85 μm
V	Moderate to very steep red slope shortward of 0.7 μm with a deep absorption longward of 0.75 μm
X	Generally featureless spectrum, with a slight to moderate reddish slope
Xc	Slightly reddish spectrum, generally featureless except for a gentle curvature
Xe	Slightly to moderately red slope with a series of subtle absorption features such as one shortward of 0.55 μm
Xk	Moderately red slope shortward of about 0.75 μm, and generally flat longward of 0.75 μm

Note. This table is adapted from one in Bus and Binzel (2002b).

As stated earlier, SMASS II data were not available for all objects observed and presented here. In these cases, the taxonomic type tabulated in Appendix A includes "(SMASS I)" if the visible data are from SMASS I (Xu *et al*. 1995) or "(ECAS)" if the data are from the Eight-Color Asteroid Survey (Zellner *et al*. 1985). For both of these alternate cases, the taxonomic type indicated is based almost entirely on the classification system of Tholen (1984).

The visible portions of the presented spectra are from SMASS II (Bus and Binzel 2002a), except as noted in Appendix A. No systematic variations (Burbine 2000) in slope, from comparisons of the reflectance values at 1.65 μm, were seen between the SMASSIR and 52-color data sets. It should be noted that since all spectra are normalized to a visible spectrum, slope differences between previously taken spectra and SMASSIR spectra could be due to differences in the visible and/or the near-infrared spectra.

RESULTS

The following sections discuss the results of the SMASSIR survey for A, K, and O asteroids and the Vestoids (objects with visible spectra similar to Vesta). Analyses of the spectra of these objects appear to be the least hampered by the lack of spectral coverage out to 2.5 μm. A and K asteroids have spectral features shortward of $\sim$1.65 μm due to olivine while Vestoids have spectral features due to pyroxene in this wavelength range. The O asteroid discussed here has an unusual spectrum shortward of $\sim$1.65 μm.

The S asteroids are difficult to analyze using SMASSIR spectra since their absorption features are primarily due to mixtures of olivine and pyroxene. The olivine and pyroxene features overlap in the 1-μm wavelength region, making it difficult to make mineralogical interpretations without wavelength coverage out to 2.5 μm. The usefulness of much of the SMASSIR spectra of S asteroids may be in identifying unusual objects to be observed out to 2.5 μm and confirming the spectral characteristics (out to $\sim$1.65 μm) of objects observed in the near-infrared.

A Asteroids

A-class asteroids have strong UV and 1-μm features that appear similar to those of olivine [$(Mg, Fe)_2SiO_4$] (e.g., Cruikshank and Hartmann 1984). Nine main-belt A-class asteroids were observed in SMASSIR. All of these objects were classified as A types in the Bus and Binzel (2002b) taxonomy.

Mineralogically significant parameters for these objects derived from SMASSIR spectra are given in Table II. These objects can be divided into two groups. The larger (diameters of 27 to 60 km) A types (246 Asporina, 289 Nenetta, 446 Aeternitas, and 863 Benkoela) (Fig. 1), previously observed by Bell *et al.* (1988), have distinctive absorption bands due to olivine. The smaller and newly identified A-type asteroids (1126 Otero, 1600 Vyssotsky, 2732 Witt, 4142 Dersa-Uzala, and 4713 Steel) (Fig. 2) have much weaker 1-μm bands. The smaller A asteroids have estimated diameters of 13 km or less.

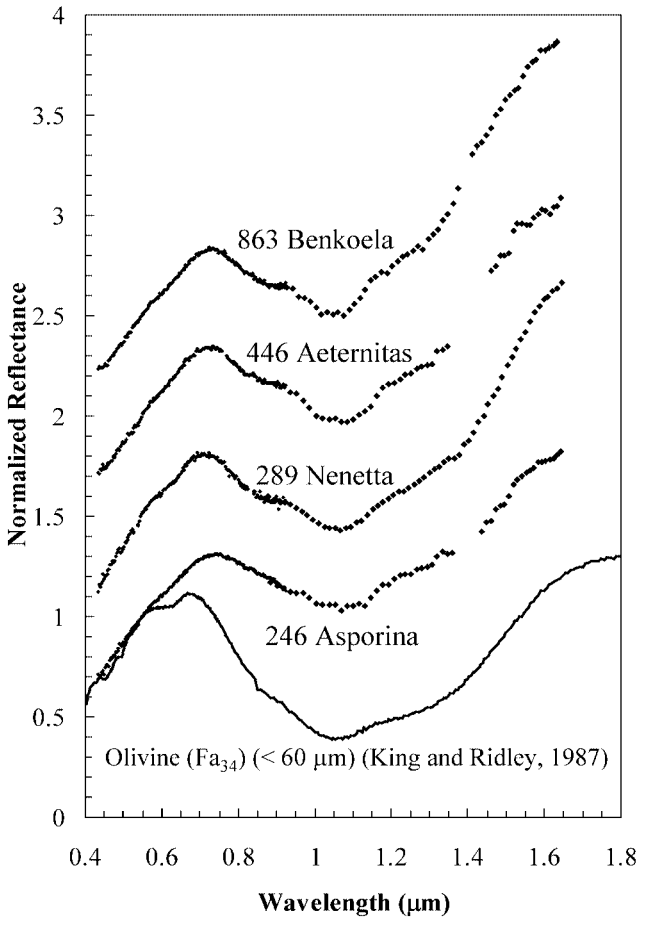

FIG. 1. Reflectance spectra of four deep-featured A-type asteroids and olivine from King and Ridley (1987). The A-type asteroids can be seen to have band depths similar to those of the olivine spectrum, but much redder spectral slopes. All spectra are normalized to unity at 0.55 μm and all of the asteroid spectra have been offset in reflectance by 0.5.

One object, Steel, has been classified as an S-type asteroid by Carvano *et al.* (2001). They observed it over two nights and noted that it did not have a strong UV feature, as seen in their spectrum of Vyssotsky. Further observations of this object are needed to confirm the visible spectral characteristics of this object.

The deep-featured objects are also much redder than most known olivine from extraterrestrial or terrestrial sources (Table II). These asteroids have reflectances at 1.65 μm (normalized to unity at 0.55 μm) between $\sim$1.80 and $\sim$2.4. An olivine spectrum plotted by Adams (1975) labeled with a fayalite (Fa) content of 100 mol% and one by Sunshine and Pieters (1998) with a Fa_{99} composition appear as red as these A asteroids. The spectrum of Fa_{89} olivine by King and Ridley (1987) is not as red as these asteroids (Table II).

Olivine-dominated meteorites, such as the brachinites ($\sim Fa_{30-35}$) and pallasites ($\sim Fa_{10-20}$), have much lower iron contents (Mittlefehldt *et al.* 1998). An olivine grain in one eucrite has been found to very iron-rich (Fa_{83}) (Mittlefehldt and Lindstrom 1993) and some almost-pure fayalite grains that are 100 μm or less in size have been identified in some CV chondrites

TABLE II
Band Positions and Depths for 1-μm Features of A-Type Asteroids, Meteorites, Olivine, and Olivine/Metal Mixtures

	~0.7 μm peak (μm)[a]	Band minimum (μm)[a]	Band center (μm)[a]	Band depth[b]	Albedo[c]	Reflectance at 1.65 μm[d]	Diameter (km)[e]
Asteroid							
246 Asporina	0.74	1.07	1.10	35%	0.17	1.82	60
289 Nenetta	0.71	1.07	1.09	54%	0.24	2.17	34
446 Aeternitas	0.73	1.08	1.09	48%	0.24	2.09	45
863 Benkoela	0.73	1.07	1.08	54%	0.60	2.37	27
1126 Otero	0.74	0.94	1.07	17%	0.18	1.50	12
1600 Vyssotsky	0.74	0.91	1.04	16%	—	1.47	(13)
2715 Mielikki	0.75	1.02	1.06	18%	0.18	1.57	13
2732 Witt	0.74	0.89	(0.90)[f]	11%	—	1.55	(12)
4142 Dersa-Uzala	0.74	0.90	1.05	22%	—	1.84	(6)
4713 Steel	0.74	0.92	0.92	14%	—	1.64	(9)
Meteorites[g]							
Brachina	0.68	1.05	1.06	67%	0.29	1.33	
Brenham	0.68	1.05	1.05	32%	0.59	1.15	
Imilac	0.68	1.08	1.08	40%	0.13	1.14	
Olivine[h]							
Fa_{12} (300 K)	0.57	1.05	1.06	67%	0.63	1.14	
Fa_{12} (120 K)	0.57	1.05	1.05	70%	0.65	1.16	
Fa_{34}	0.67	1.06	1.07	70%	0.44	1.19	
Fa_{40}	0.67	1.06	1.08	66%	0.46	1.21	
Fa_{49}	0.67	1.07	1.08	63%	0.38	1.22	
Fa_{89}	0.69	1.07	1.08	74%	0.27	1.40	
Altered olivine by pulse laser irradiation (Yamada *et al.* 1999)[i]							
Fa_9 (unaltered)	0.57	1.06	1.06	37%	0.87	1.07	
Fa_9 (15 mJ laser)	0.71	1.06	1.07	36%	0.59	1.43	
Fa_9 (30 mJ laser)	0.73	1.05	1.07	34%	0.46	1.78	
Melted and recrystallized olivine (Moroz *et al.* 1996)[i]							
Fa_{10} (unaltered)	0.56	1.06	1.06	47%	0.73	1.08	
Fa_{10} (partially)	0.69	1.05	1.06	40%	0.49	1.35	
Fa_{10} (altered)	0.75	1.07	1.06	14%	0.24	1.09	
Olivine and metal (Cloutis *et al.* 1990)							
100% olivine	0.56	1.05	1.05	70%	0.72	1.07	
75% olivine; 25% metal	0.69	1.05	1.05	36%	0.26	1.20	
50% olivine; 50% metal	0.89	1.04	1.05	13%	0.16	1.49	
100% metal	—	—	—	0%	0.11	2.00	

[a] The estimated error bars for the asteroid band positions are $\pm$0.01 μm for the ~0.7-μm peak. The estimated error bars for the band minima and centers (minima where a linear continuum has been divided out) are $\pm$0.01 μm for the higher quality A-asteroid spectra (246 Asporina, 289 Nenetta, 446 Aeternitas, 863 Benkoela) and $\pm$0.02 μm for the lower quality spectra (1126 Otero, 1600 Vyssotsky, 2715 Mielikki, 2732 Witt, 4142 Dersa-Uzala, 4713 Steel). The estimated error bars for band positions from the olivine spectra are estimated to be $\pm$0.01 μm.

[b] The estimated error bars for the band depths are $\pm$5% times the depth. The band depth is calculated after a linear continuum of each spectrum is divided out.

[c] The asteroid albedos are IRAS albedos (http://pdssbn.astro.umd.edu/SBNast/archive/IMPS/diamalb.tab). The albedos of the meteorites, the olivine, and olivine/metal mixtures are their reflectances at 0.55 μm.

[d] The error bars for the reflectances at 1.65 μm for the asteroids are $\pm$5%.

[e] The asteroid diameters without parentheses are from IRAS. The asteroid diameters in parentheses are calculated from the H magnitude (Bowell *et al.* 1989) assuming an albedo of 0.18.

[f] The relatively short wavelength for the band center for 2732 Witt appears to be due to problems in overlapping the SMASS and SMASSIR data at 0.92 μm and the scatter in the SMASSIR spectra.

[g] The parameters for the Brachina spectrum are from Sunshine and Hiroi (personal communication 1998), the Imilac olivine spectrum are from Hiroi *et al.* (1993), and the Brenham olivine spectrum are from King and Ridley (1987).

[h] The spectra of the Fa_{12} olivine taken at two different temperatures are from Hinrichs *et al.* (1999) and the spectra of the Fa_{34}, Fa_{40}, Fa_{49}, and Fa_{89} olivine are from King and Ridley (1987).

[i] The olivines altered by Yamada *et al.* (1999) and Moroz *et al.* (1996) were irradiated by a laser with the Yamada *et al.* (1999) samples being altered at lower energies with shorter durations.

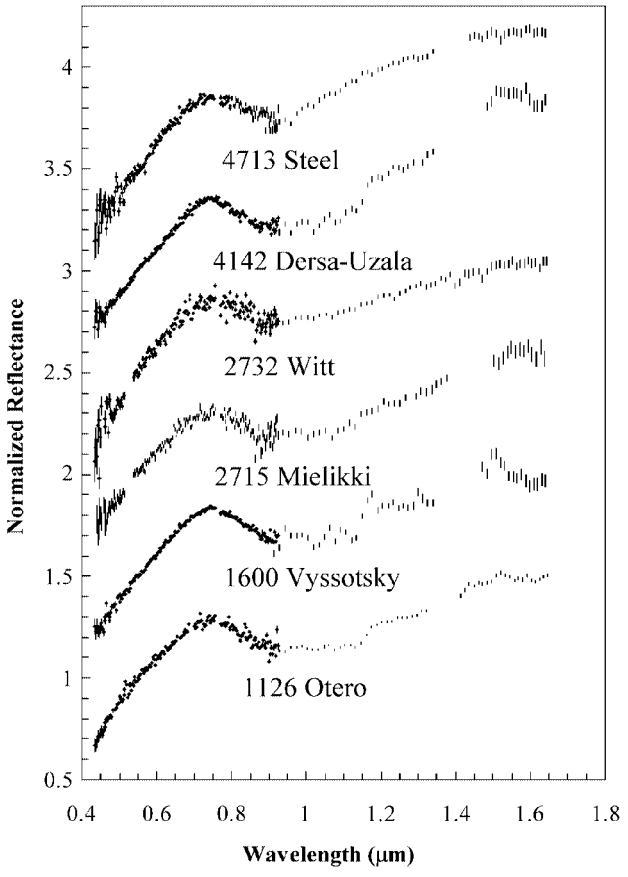

FIG. 2. Reflectance spectra of weaker featured A-types. All spectra are normalized to unity at 0.55 μm and all of the asteroid spectra have been offset in reflectance by 0.2.

(Hua and Buseck 1995). But olivine compositions of Fa_{40} or higher tend to be very rare in meteorites (Brearley *et al*. 1998, Mittlefehldt *et al.* 1998). We find no meteoritical evidence to support the formation of kilometer-sized bodies with compositions close to Fa_{100}.

One proposed way to alter a surface to keep these objects' strong UV features and strong distinctive bands due to olivine while reddening the spectra is to use a pulse laser (Sasaki *et al.* 2001), which is hoped to duplicate the energy and duration of micrometeorite impacts. We find it intriguing that the altered olivine samples appear more spectrally similar to A-asteroid spectra than any other known samples.

One possibility for the surface composition of the shallower featured A asteroids (such as 1126 Otero) is that they are mixtures of metal and silicates (olivine and/or pyroxene) that would be expected to have very broad, but shallow 1-μm bands. Another possibility is that they have been more heavily "altered," which should tend to suppress the 1-μm feature, than the deep-featured A asteroids.

Within the A-asteroid population defined by Bus and Binzel (2002b), it appears that objects with the distinctive bands due to olivine tend to be prevalent only at rather large diameters (27 to 60 km). A-type asteroids in the Bus and Binzel (2002b) taxonomy include a number of objects with different near-infrared spectral properties. The spectral differences between the large and small A asteroids could be due to composition and/or "alteration" effects. Larger objects would be expected to have older surfaces and be more altered than smaller asteroids, which would argue that the spectral differences are more likely due to some type of compositional difference.

K Asteroids

K-types asteroids have been noted (e.g., Bell 1988) as having visible and near-infrared spectra similar to those of CO3/CV3 chondrites; however, previous near-infrared spectra (Bell *et al.* 1988) of these asteroids are rather noisy with large amounts of scatter. Nine main-belt K asteroids were observed in SMASSIR. All of these objects were classified as K types in the Bus and Binzel (2002b) taxonomy. Spectra of three K asteroids were previously discussed in Burbine *et al.* (2001a).

Five of these objects (221 Eos, 513 Centesima, 653 Berenike, 661 Cloelia, and 1148 Rarahu) are in the hierarchical clustering method (HCM) Eos family (Zappalà *et al.* 1995) and four of the asteroids (233 Asterope, 402 Chloe, 599 Luisa, and 7081 Ludibunda) are not.

As discussed in Burbine *et al.* (2001a) for two objects (Eos and Berenike), the Eos family members (Fig. 3) (excluding 1148 Rarahu) tend to have spectra similar to that of CO3 chondrite Warrenton (Gaffey 1976). (The near-infrared spectrum of Cloelia is noisy but seems to have similar spectral characteristics.) These objects have UV features with similar strengths, plus an absorption feature with band depths of ~10% centered around 1.06–1.09 μm. The wavelength position of this feature plus the more subtle features at ~0.9 and ~1.3 μm indicates an olivine-dominated assemblage where the olivine bands are suppressed in strength due to an opaque substance (e.g., metallic iron, sulfide, carbon). Warrenton (Wahl 1950) is 75 vol% olivine (Fa_{27}; Scott and Jones 1990), 4% pyroxene, 6% metallic iron, and 5% troilite. The exception is 1148 Rarahu, whose noisy spectrum appears reddened relative to those of the other Eos family members. However, the spectrum of Rarahu does appear to indicate an olivine-dominated assemblage so it is unclear if Rarahu is an interloper or an olivine-dominated fragment of the original "Eos family" parent body that has been reddened by some process.

Three of the K asteroids (233 Asterope, 402 Chloe, and 599 Luisa) not in the Eos family tend to have much weaker 1-μm absorption features and a variety of spectral slopes (Fig. 4). Tholen (1984) originally classified Asterope as a T-type asteroid. Burbine *et al.* (2001a) noted the spectral similarity of Luisa and CV3 chondrite Mokoia (Gaffey 1976). The exception is 7081 Ludibunda, whose noisy spectrum (Fig. 4) has a much deeper 1-μm band that is similar to the spectra of the Eos family members. Ludibunda is located at ~2.74 AU, relatively far from the Eos family at ~3 AU. As with the A asteroids, K-type objects in the Bus and Binzel (2002b) taxonomy include

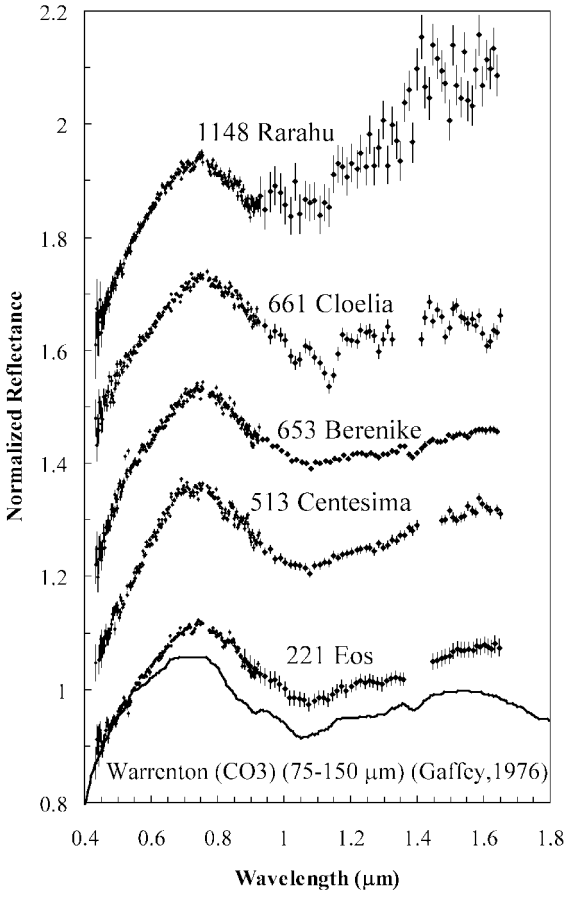

FIG. 3. Reflectance spectra of K asteroids in the Eos family and CO3 chondrite Warrenton from Gaffey (1976). The Warrenton spectrum has had a nonlinear correction factor (Pieters and Pratt, personal communication 2001) added to the original wavelengths to compensate for a later discovered calibration offset (Gaffey 1984). All spectra are normalized to unity at 0.55 μm and all of the asteroid spectra have been offset in reflectance by 0.2.

a number of objects with very different near-infrared spectral properties.

O Asteroid

One main-belt O asteroid (3628 Božněmcová) was observed in SMASSIR. This object was originally announced (Binzel *et al.* 1993) as the first main-belt object with a visible spectrum similar to those of ordinary chondrites. However, near-infrared spectra of Božněmcová (Fig. 5) show an unusual bowl-shaped 1-μm feature that is unlike any individual ordinary chondrite or other currently measured meteorite spectrum from $\sim$0.5 to $\sim$1.5 μm.

The large error bars for this spectrum are due to its faint magnitude of V17.1. As can be seen in the figure, Božněmcová matches very well the Manbhoom spectrum from 0.6 to 1.1 μm, but deviates from Manbhoom between 1.1 and 1.4 μm. One possibility is that atmospheric absorption features are affecting the spectrum between these wavelengths and causing the deviation. However, problems due to the atmosphere would need to happen at a much shorter wavelength ($\sim$1.30 μm) than is normally found. Also, Božněmcová's spectrum is very smooth without significant scatter as would be expected for a substantial atmospheric correction problem.

Božněmcová's band center near 1 μm is too long to indicate a surface dominated by orthopyroxene and too short to indicate an olivine-dominated surface. One possibility is an olivine-orthopyroxene mixture (e.g., Cloutis *et al.* 1986) or a substantial high Ca-pyroxene component (Cloutis and Gaffey 1991). Spectra out to 2.5 μm for this object may be critical for making an educated guess on the surface composition of this object.

Vestoids

Asteroid 4 Vesta has been postulated (e.g., McCord *et al.* 1970, Larson and Fink 1975, Consolmagno and Drake 1977) as the parent body of the howardites, eucrites, and diogenites (HEDs)

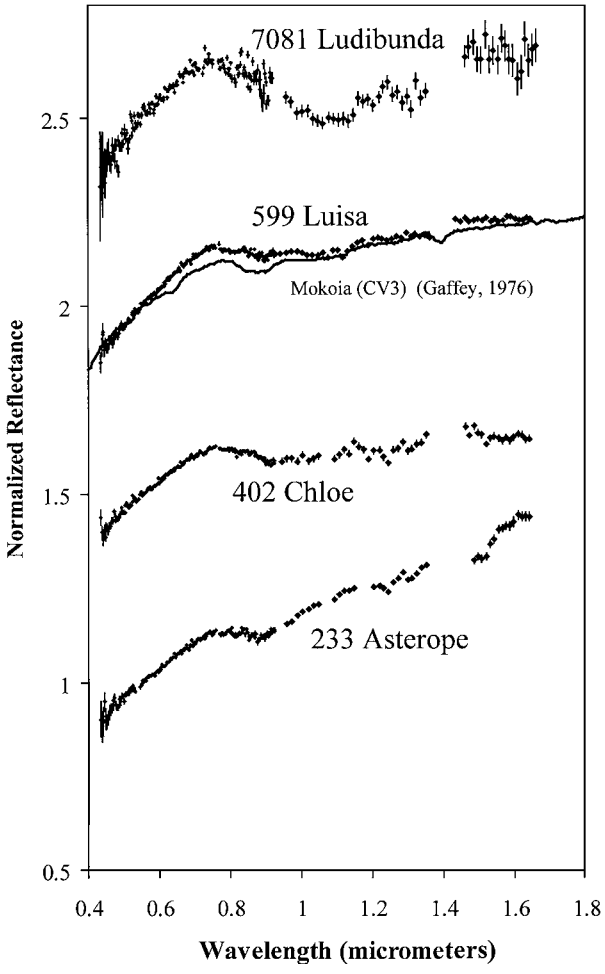

FIG. 4. Reflectance spectra of K asteroids not in the Eos family and CV3 chondrite Mokoia from Gaffey (1976). The Mokoia spectrum has had a nonlinear correction factor (Pieters and Pratt, personal communication 2001) added to the original wavelengths to compensate for a later discovered calibration offset (Gaffey 1984). All spectra are normalized to unity at 0.55 μm and all of the asteroid spectra have been offset in reflectance by 0.5.

TABLE III
Vestoids Observed in SMASSIR

Asteroid	Class[a] (SMASS II)	Proper elements[b] a'	e'	$\sin i'$	HCM family[c]
4 Vesta	V	2.362	0.099	0.111	Vesta
1273 Helma	V(SMASS I)	2.394	0.123	0.109	
1459 Magnya	V	3.150	0.218	0.265	
1906 Naef	V(SMASS I)	2.374	0.100	0.112	Vesta
1929 Kollaa	V	2.363	0.114	0.123	Vesta
1933 Tinchen	V(SMASS I)	2.353	0.094	0.119	Vesta
2045 Peking	V	2.380	0.090	0.116	Vesta
2442 Corbett	J(SMASS I)	2.388	0.097	0.095	
2579 Spartacus	V	2.210	0.081	0.103	
2590 Mourào	V(SMASS I)	2.343	0.097	0.117	Vesta
2653 Principia	V	2.444	0.115	0.089	
2763 Jeans	V	2.404	0.179	0.075	
2851 Harbin	V	2.478	0.120	0.136	
3268 De Sanctis	V(SMASS I)	2.347	0.100	0.122	Vesta
3376 Armandhammer	Sq	2.349	0.097	0.123	Vesta
3657 Ermolova	J(SMASS I)	2.313	0.085	0.115	Vesta
3849 Incidentia	V	2.474	0.065	0.094	
3944 Halliday	V(SMASS I)	2.368	0.109	0.118	Vesta
3968 Koptelov	V(SMASS I)	2.322	0.091	0.116	Vesta
4005 Dyagilev	J(SMASS I)	2.452	0.113	0.105	Vesta
4147 Lennon	V(SMASS I)	2.362	0.102	0.113	Vesta
4188 Kitezh	V	2.335	0.112	0.098	
4215 Kamo	V	2.417	0.098	0.115	Vesta
4311 Zguridi	V	2.442	0.110	0.109	Vesta
4900 Maymelou	V	2.379	0.102	0.114	Vesta

[a] Classes are from SMASS II (Bus and Binzel 2002b) unless noted by SMASS I, where the class is from data of Xu *et al.* (1995).

[b] Proper elements are from an update compilation (http://hamilton.dm.unipi.it/astdys/catalogs/allnum.pro) of Milani and Knežević (1994) proper elements.

[c] Family memberships are from an updated compilation (http://www.obs-nice.fr/cerga/HCM.DAT) of Zappalà *et al.* (1995) family memberships.

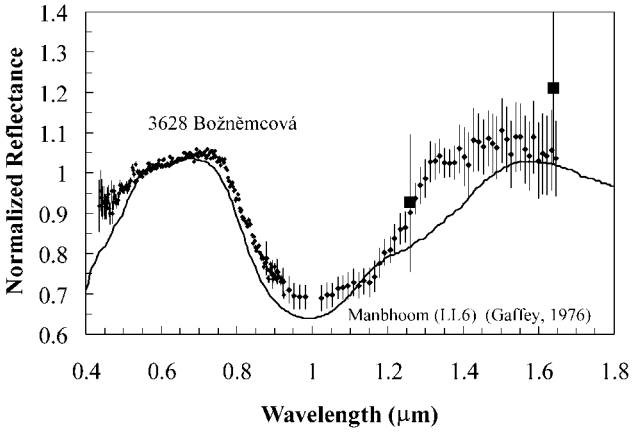

FIG. 5. Reflectance spectra of 3628 Božněmcová and LL6 chondrite Manbhoom from Gaffey (1976). The large squares are the J and H filter band measurements reported by Binzel *et al.* (1993) showing their agreement (within error bars) of the SMASSIR measurements. The Manbhoom spectrum has had a nonlinear correction factor (Pieters and Pratt, personal communication 2001) added to the original wavelengths to compensate for a later discovered calibration offset (Gaffey 1984). All spectra are normalized to unity at 0.55 μm.

due to Vesta's distinctive reflectance spectrum, which is similar in structure to the laboratory spectra of HEDs. Binzel and Xu (1993), Xu *et al.* (1995), and Bus (1999) identified a number of small asteroids with "Vesta-like" visible spectra (usually called Vestoids). (We use the term "Vestoid" for objects with visible spectra similar to those of Vesta and/or the HEDs, even if they are not believed to be fragments of Vesta.) Vestoids were found in the Vesta family and between Vesta and meteorite-supplying resonances such as the 3 : 1 (~2.5 AU) and ν_6, supporting the argument that HEDs are fragments of Vesta. One outer main-belt Vestoid has been discovered by Lazzaro *et al.* (2000).

Twenty-five main-belt Vestoids (V and J asteroids plus the Sq object 3376 Armandhammer in the Vesta family) (Table III) were observed in SMASSIR. Most of these objects have

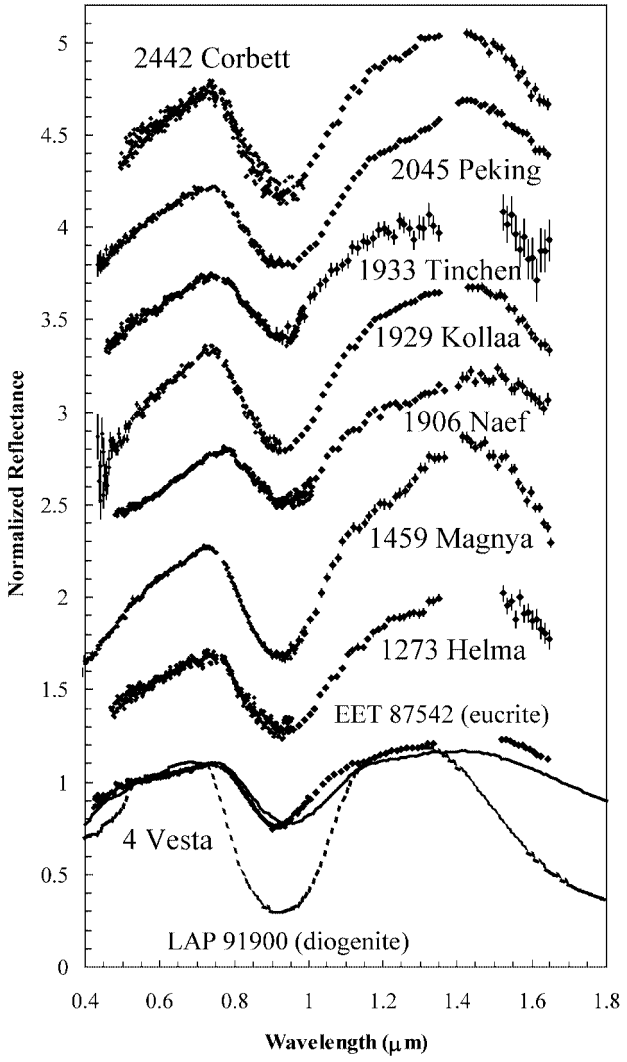

FIG. 6. Reflectance spectra of eight Vestoids, the eucrite EET 87542 (bold line) (Burbine *et al.* 2001a), and the diogenite LAP 91900 (dashed line). The turnover between the 1- and 2-μm feature for the Vestoids is at a wavelength similar to those of the eucrites and at a much longer wavelength than the diogenite. All spectra are normalized to unity at 0.55 μm and all of the asteroid spectra have been offset in reflectance by 0.5.

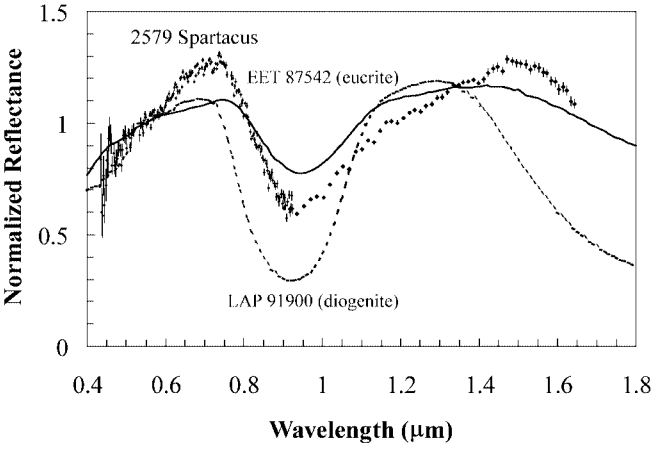

FIG. 7. Reflectance spectra of 2579 Spartacus, the eucrite EET 87542 (bold line) (Burbine *et al.* 2001a), and the diogenite LAP 91900 (dashed line). The spectrum of Spartacus appears to have an olivine component that has broadened its 1-μm feature and lengthened the turnover ($\sim$1.5 μm) relative to other Vestoids. All spectra are normalized to unity at 0.55 μm.

been discussed previously (Lazzaro *et al.* 2000, Burbine *et al.* 2001b) so we only summarize the major conclusions of these studies.

Twenty-four of these objects (all except 2579 Spartacus) have the distinctive 1-μm feature due to pyroxene plus the start of the 2-μm feature also due to pyroxene. Of these 24 objects, 16 were in the HCM Vesta family (Zappalà *et al.* 1995).

Representative spectra of eight of these objects are plotted in Fig. 6 versus a eucrite and a diogenite. Their absorption bands are similar to those found in eucrites and also howardites (breccias of eucritic and diogenitic material). None of the objects have spectra that resemble those of diogenites, whose turnover between the 1 and 2-μm features is at a wavelength much shorter than those of the measured Vestoids. The observed objects have spectra redder (higher reflectances at wavelengths longward of 1 μm) than Vesta's, which is consistent with their pyroxenes being more Ca-rich than the average pyroxenes on Vesta's surface (Burbine *et al.* 2001b). Spectral observations of one Vestoid (1929 Kollaa) out to 2.5 μm by Kelley *et al.* (2001a) and mineralogical analyses of its spectrum confirm a similarity to eucrites.

The exception is the spectrum of 2579 Spartacus (Fig. 7), which appears to have either an olivine or a high-Ca pyroxene component that has broadened its 1-μm feature and lengthened the turnover ($\sim$1.5 μm) relative to other Vestoids. Spartacus is located ($\sim$2.2 AU) at a relatively large ejection velocity ($\sim$1 km/s) from Vesta at $\sim$2.34 AU and it is unclear if $\sim$10-km fragments could be ejected at those velocities (Asphaug 1997). Spectra out to 2.5 μm are needed to better determine Spartacus' surface composition.

SMASSIR observations (Lazzaro *et al.* 2000) also confirm the spectral similarity of an outer belt Vestoid (1459 Magnya) (Fig. 6) to the inner main-belt Vestoids. Magnya is located at $\sim$3.15 AU, too far to be easily related to Vesta. The discovery (Yamaguchi *et al.* 2002) of one eucrite with a very different oxygen isotopic value from the HEDs also appears to confirm the formation of other "Vesta-like" bodies in the asteroid belt.

CONCLUSIONS

The SMASSIR data set is the first extensive survey of small (diameters less than 20 km) main-belt asteroids in the wavelength range past 1 μm. However, the lack of spectral coverage out to 2.5 μm hampers making any definitive mineralogical characterization. Mineralogies can be predicted (e.g., eucrite/howardite and not diogenite surface compositions for almost all of the Vestoids) from SMASSIR data, but spectral data out to 2.5 μm are needed to confirm these predictions.

A system at the IRTF called SpeX now allows spectral observations out to 2.5 μm (e.g., Binzel *et al.* 2001b, Kelley *et al.* 2001a, 2001b). SpeX is a new-generation low-to-medium-resolution spectrograph, which is capable of producing spectra of faint asteroids from 0.8 to 2.5 μm with a signal-to-noise ratio comparable to that achieved in the visible wavelengths (Bus *et al.* 2001).

APPENDIX A

Observational Parameters for SMASSIR Objects

Asteroid	Class (SMASS II)	Date[a]	Time (UT)[a]	Airmass[b]	Number of images[c]	Standard star[d]	Airmass[b]
1 Ceres	C	09/15/98	15:25–15:30	1.00	8	Hyades 64	1.00
2 Pallas	B	09/18/98	09:49–09:53	1.09	10	112-1333	1.10
3 Juno	Sk	01/04/98	15:45–15:52	1.09	6	Hyades 64	1.04
4 Vesta[e]	V(SMASS I)	01/30/97	14:17–14:25	1.35	7	Hyades 64	1.03
5 Astraea	S	03/01/99	05:19–05:25	1.06	6	Hyades 64	1.06
6 Hebe	S	05/02/98	13:24–13:30	1.09	6	107-998	1.10
7 Iris	S	02/08/97	15:17–15:23	1.27	6	Hyades 64	1.01
9 Metis	S(ECAS)	03/01/99	13:57–14:02	1.13	8	102-1081	1.07
10 Hygiea	C	01/04/98	09:24–09:35	1.04	10	Hyades 64	1.04
11 Parthenope	Sk	10/02/97	14:20–14:28	1.14	10	Hyades 64	1.05
12 Victoria	L	01/27/99	14:29–14:40	1.21	10	Hyades 64	1.12
13 Egeria	Ch	12/05/99	09:19–09:56	1.12	18	Hyades 64	1.01
14 Irene	S	12/05/99	12:54–13:06	1.02	8	Hyades 64	1.01

APPENDIX A—*Continued*

Asteroid	Class (SMASS II)	Date[a]	Time (UT)[a]	Airmass[b]	Number of images[c]	Standard star[d]	Airmass[b]
15 Eunomia	S	09/16/98	14:14–14:20	1.04	6	Hyades 64	1.00
16 Psyche	X	04/30/98	11:25–11:30	1.25	6	102-1081	1.11
18 Melpomene	S	05/02/98	13:35–13:40	1.10	6	107-998	1.10
19 Fortuna	Ch	02/27/99	09:37–09:45	1.01	6	Hyades 64	1.01
20 Massalia	S	09/16/98	14:04–14:19	1.04	6	93-101	1.09
21 Lutetia	Xk	01/05/98	12:04–12:10	1.03	10	102-1081	1.20
22 Kalliope	X	02/08/97	06:26–06:32	1.03	6	Hyades 64	1.01
25 Phocaea	S	02/08/97	08:58–09:11	1.16	10	Hyades 64	1.01
26 Proserpina	S	03/01/99	06:00–06:06	1.03	6	Hyades 64	1.06
28 Bellona	S	02/10/97	08:09–08:16	1.04	6	Hyades 64	1.01
32 Pomona	S	04/30/98	10:06–10:20	1.22	10	102-1081	1.11
33 Polyhymnia	Sq	02/09/97	09:48–09:59	1.04	10	Hyades 64	1.01
37 Fides	S	05/24/99	07:19–07:35	1.13	10	102-1081	1.09
39 Laetitia	S	01/05/98	10:40–10:55	1.07	10	102-1081	1.20
40 Harmonia	S	10/02/97	11:27–11:34	1.50	10	93-101	1.07
42 Isis	L	02/09/97	15:33–15:43	1.17	10	Hyades 64	1.01
43 Ariadne	Sk	02/08/97	09:28–09:39	1.01	6	Hyades 64	1.01
44 Nysa	Xc	09/15/98	13:32–13:37	1.06	10	93-101	1.08
57 Mnemosyne	S	02/08/97	15:30–15:42	1.21	10	Hyades 64	1.01
63 Ausonia	Sa	02/09/97	05:31–05:37	1.11	6	Hyades 64	1.01
64 Angelina	Xe	02/08/97	12:45–13:02	1.05	5	Hyades 64	1.01
65 Cybele	Xc	02/28/99	06:03–06:10	1.02	8	Hyades 64	1.08
68 Leto	S(SMASS I)	10/02/97	14:40–14:48	1.17	10	Hyades 64	1.05
71 Niobe	Xe	09/17/98	05:36–05:47	1.34	5	112-1333	1.13
73 Klytia	S(SMASS I)	12/06/98	08:17–08:29	1.02	8	Hyades 64	1.01
76 Freid	X	08/11/99	09:31–09:55	1.24	10	112-1333	1.08
80 Sappho	S	10/02/97	15:21–15:28	1.11	8	Hyades 64	1.05
82 Alkmene	Sq	10/02/97	14:54–15:05	1.17	8	Hyades 64	1.05
92 Undina	Xc	04/30/98	14:11–14:36	1.29	8	102-1081	1.11
103 Hera	S	05/06/00	09:10–09:31	1.08	12	102-1081	1.07
106 Dione	Cgh	12/06/99	14:40–14:54	1.00	8	Hyades 64	1.01
113 Amalthea	S	10/02/97	12:23–12:39	1.09	10	93-101	1.09
114 Kassandra	Xk	12/05/99	08:39–08:52	1.05	10	Hyades 64	1.01
122 Gerda	L	08/11/99	10:18–10:29	1.19	10	112-1333	1.08
126 Velleda	S(SMASS I)	03/04/00	11:27–11:47	1.10	10	102-1081	1.07
130 Elektra	Ch	05/07/00	07:55–08:19	1.04	12	102-1081	1.07
140 Siwa	Xc	01/04/98	12:10–12:46	1.05	10	Hyades 64	1.05
158 Koronis	S	05/01/98	06:25–06:33	1.02	10	107-998	1.06
167 Urda	Sk	10/03/97	11:49–12:01	1.08	10	93-101	1.06
169 Zelia	Sl	02/10/97	07:07–07:17	1.06	10	Hyades 64	1.01
221 Eos	K	04/29/98	10:43–11:01	1.06	10	102-1081	1.07
233 Asterope	K	05/06/00	08:40–09:02	1.16	10	102-1081	1.07
236 Honoria	L	12/05/99	14:53–15:10	1.00	10	Hyades 64	1.00
243 Ida	S	02/10/97	08:25–08:39	1.05	10	Hyades 64	1.01
244 Sita	Sa	05/22/99	13:50–14:14	1.25	10	102-1081	1.25
246 Asporina	A	10/02/97	10:30–10:41	1.35	10	93-101	1.07
253 Mathilde	Cb	01/04/98	08:05–08:45	1.17	18	Hyades 64	1.04
289 Nenetta	A	02/09/97	10:27–10:42	1.02	10	Hyades 64	1.01
291 Alice	S(SMASS I)	10/02/97	10:50–11:08	1.32	16	93-101	1.07
304 Olga	Xc	10/03/97	13:42–13:53	1.07	10	93-101	1.06
308 Polyxo	T	12/05/99	15:24–15:40	1.03	10	Hyades 64	1.01
317 Roxane	Xe	12/06/99	11:56–12:08	1.01	8	Hyades 64	1.01
335 Roberta	B	10/03/97	11:18–11:27	1.26	8	93-101	1.06
336 Lacaderia	Xk	02/28/99	11:01–11:09	1.09	8	Hyades 64	1.08
346 Hermentaria	S	02/08/97	13:27–13:33	1.01	6	Hyades 64	1.01
349 Dembowska	R	01/04/98	09:08–09:25	1.10	10	Hyades 64	1.04
352 Gisela	Sl	02/10/97	10:14–10:25	1.08	10	Hyades 64	1.01
354 Eleonora	Sl	02/09/97	15:50–15:58	1.22	10	Hyades 64	1.01
364 Isara	S(ECAS)	03/01/99	12:54–13:16	1.05	14	Hyades 64	1.06
374 Burgundia	S	05/24/99	14:30–14:43	1.13	8	102-1081	1.09

APPENDIX A—*Continued*

Asteroid	Class (SMASS II)	Date[a]	Time (UT)[a]	Airmass[b]	Number of images[c]	Standard star[d]	Airmass[b]
379 Huenna	C	03/01/99	05:39–05:53	1.06	8	Hyades 64	1.06
389 Industria	S	10/01/97	11:42–11:53	1.15	10	93-101	1.15
402 Chloe	K	08/11/99	13:10–13:25	1.14	10	112-1333	1.08
416 Vaticana	Sl	02/10/97	07:24–07:38	1.10	10	Hyades 64	1.01
431 Nephele	B	03/03/00	14:00–14:19	1.17	10	102-1081	1.06
446 Aeternitas	A	10/01/97	13:14–13:34	1.00	10	93-101	1.06
458 Hercynia	L	12/06/99	12:23–12:36	1.02	8	Hyades 64	1.01
470 Kilia	S	08/11/99	12:07–12:23	1.13	8	112-1333	1.08
477 Italia	S	12/06/99	09:35–09:54	1.04	8	Hyades 64	1.01
478 Tergeste	L	08/11/99	07:13–07:29	1.30	10	112-1333	1.08
480 Hansa	S(SMASS I)	10/03/97	13:21–13:32	1.10	10	93-101	1.06
509 Iolanda	S	05/06/00	12:57–13:32	1.20	10	102-1081	1.07
511 Davida	C	05/24/99	09:30–09:40	1.10	8	102-1081	1.09
513 Centesima	K	03/02/00	10:03–10:28	1.05	10	102-1081	1.07
515 Athalia	Cb	03/01/99	08:48–08:58	1.02	10	Hyades 64	1.06
554 Peraga	Ch	12/06/01	11:30–11:44	1.01	8	Hyades 64	1.01
562 Salome	S(ECAS)	05/07/00	11:51–12:20	1.32	10	102-1081	1.07
584 Semiramis	Sl	02/09/97	05:50–05:55	1.06	6	Hyades 64	1.01
599 Luisa	K	05/02/98	08:32–08:42	1.04	6	102-1081	1.08
611 Valeria	L	12/05/99	10:36–10:49	1.05	10	Hyades 64	1.01
625 Xenia	Sa	04/30/98	08:44–09:21	1.01	20	102-1081	1.11
653 Berenike	K	01/04/98	13:14–13:29	1.05	10	Hyades 64	1.05
661 Cloelia	K	08/10/99	10:23–10:42	1.27	10	112-1333	1.06
675 Ludmilla	S	05/01/98	07:04–07:10	1.15	6	107-998	1.06
702 Alauda	B	03/01/99	09:07–09:13	1.06	10	Hyades 64	1.06
714 Ulula	S(ECAS)	05/05/00	10:57–11:19	1.31	10	102-1081	1.07
720 Bohlinia	Sq	05/02/98	13:01–13:11	1.40	8	107-998	1.10
737 Arequipa	S	02/10/97	08:48–08:58	1.04	10	Hyades 64	1.01
753 Tiflis	L	12/05/99	07:10–07:23	1.15	8	Hyades 64	1.01
773 Irmintraud	T	02/09/97	10:55–11:07	1.01	10	Hyades 64	1.01
774 Armor	S(SMASS I)	09/16/98	14:27–14:40	1.00	10	Hyades 64	1.00
787 Moskva	S(SMASS I)	03/01/99	14:18–14:48	1.16	18	102-1081	1.07
808 Merxia	Sq	10/03/97	14:18–14:28	1.01	10	93-101	1.06
811 Nauheima	S(SMASS I)	05/02/98	12:33–12:52	1.29	10	107-998	1.10
825 Tanina	S	03/01/99	11:53–12:15	1.08	14	Hyades 64	1.06
863 Benkoela	A	04/30/98	09:34–09:53	1.02	10	102-1081	1.11
913 Otila	Sa	09/15/98	14:12–14:31	1.01	9	Hyades 64	1.00
915 Cosette	S(SMASS I)	02/28/99	07:26–07:44	1.06	12	Hyades 64	1.08
918 Itha	S(SMASS I)	10/02/97	13:32–13:51	1.07	10	93-101	1.07
950 Ahrensa	Sa	04/29/98	13:31–14:11	1.02	20	102-1081	1.07
951 Gaspra	S	03/02/00	09:28–09:47	1.03	10	102-1081	1.07
980 Anacostia	L	12/05/99	13:15–13:34	1.01	10	Hyades 64	1.01
1126 Otero	A	05/01/98	08:32–09:14	1.21	10	107-998	1.06
1148 Rarahu	K	12/06/99	12:50–13:07	1.02	8	Hyades 64	1.01
1273 Helma	V(SMASS I)	04/30/98	10:50–11:17	1.44	14	102-1081	1.11
1284 Latvia	L	03/03/00	12:11–12:35	1.22	12	102-1081	1.07
1289 Kutaïssi	S(SMASS I)	03/01/99	11:11–11:37	1.04	10	Hyades 64	1.06
1324 Knysna	Sq	01/04/98	14:36–15:27	1.08	24	Hyades 64	1.04
1350 Rosselia	Sa	02/28/99	09:26–09:48	1.00	10	Hyades 64	1.08
1459 Magnya	V	01/15/00	08:03–08:23	1.10	10	Hyades 64	1.05
1483 Hakoila	Sq	09/18/98	09:13–09:36	1.19	12	112-1333	1.10
1518 Rovaniemi	S(SMASS I)	02/28/99	06:26–06:48	1.04	14	Hyades 64	1.08
1584 Fuji	S(SMASS I)	02/28/99	06:26–06:48	1.04	14	Hyades 64	1.08
1587 Kahrstedt	Sa	05/02/98	07:41–08:03	1.08	10	102-1081	1.08
1600 Vyssotsky	A	05/24/99	07:48–08:08	1.03	10	102-1081	1.09
1626 Sadeya	S(SMASS I)	09/18/98	05:10–05:40	1.09	7	112-1333	1.10
1658 Innes	S(SMASS I)	02/10/97	13:10–13:29	1.08	10	Hyades 64	1.01
1807 Slovakia	S	01/27/99	08:40–09:21	1.01	14	Hyades 64	1.12
1904 Massevitch	R	01/05/98	12:51–13:30	1.07	20	102-1081	1.20

APPENDIX A—*Continued*

Asteroid	Class (SMASS II)	Date[a]	Time (UT)[a]	Airmass[b]	Number of images[c]	Standard star[d]	Airmass[b]
1906 Naef	V(SMASS I)	09/17/98	14:51–15:23	1.02	12	Hyades 64	1.04
1929 Kollaa	V	02/08/97	07:45–08:36	1.05	20	Hyades 64	1.01
1933 Tinchen	V(SMASS I)	05/02/98	08:57–09:26	1.06	14	102-1081	1.08
2014 Vasilevskis	S(SMASS I)	05/24/99	09:00–09:20	1.04	10	102-1081	1.09
2038 Bistro	Sa	05/01/98	11:03–11:32	1.11	6	107-998	1.06
2045 Peking	V	02/27/99	08:43–09:25	1.01	20	102-1081	1.08
2078 Nanking	Sq	02/10/97	09:36–09:54	1.05	10	102-1081	1.07
2159 Kukkamäki	S(SMASS I)	02/10/97	06:25–06:53	1.02	12	Hyades 64	1.01
2396 Kochi	Sa	03/01/99	06:12–06:53	1.02	20	Hyades 64	1.06
2442 Corbett	J(SMASS I)	09/16/98	06:20–06:42	1.21	10	112-1333	1.07
2579 Spartacus	V	10/02/97	12:51–13:19	1.13	14	93-101	1.07
2590 Mourào	V(SMASS I)	02/09/97	08:16–08:35	1.08	10	Hyades 64	1.01
2653 Principia	V	09/15/98	11:40–12:13	1.10	16	112-1333	1.06
2715 Mielikki	A	10/03/97	14:36–15:03	1.00	14	93-101	1.06
2732 Witt	A	10/03/97	12:14–12:50	1.07	18	93-101	1.06
2763 Jeans	V	01/27/99	11:37–12:20	1.04	14	Hyades 64	1.12
2851 Harbin	V	03/01/99	09:21–09:39	1.05	10	Hyades 64	1.06
2873 Binzel	Sq	05/24/99	08:27–08:47	1.09	10	102-1081	1.09
2902 Westerlund	Sq	05/06/00	09:39–10:07	1.14	12	102-1081	1.07
3167 Babcock	S(SMASS I)	01/05/98	14:27–15:00	1.01	16	102-1081	1.20
3268 De Sanctis	V(SMASS I)	10/01/97	12:17–12:57	1.06	13	Hyades 64	1.00
3376 Armandhammer	Sq	01/04/98	11:26–11:54	1.09	14	Hyades 64	1.04
3474 Linsley	Sa	05/24/99	09:50–10:17	1.19	12	102-1081	1.09
3545 Gaffey	Sa	05/23/99	09:15–09:52	1.24	16	102-1081	1.18
3628 Božněmcová[f]	O	02/09/97	08:51–09:35	1.16	39	Hyades 64	1.01
		02/09/97	11:20–12:59	1.08	17	102-1081	1.11
3657 Ermolova	J(SMASS I)	02/09/97	07:05–07:23	1.02	12	Hyades 64	1.01
3767 DiMaggio	Sa	05/24/99	13:55–14:20	1.20	12	102-1081	1.09
3819 Robinson	Sr	04/29/98	09:28–10:22	1.13	20	102-1081	1.07
3849 Incidentia	V	03/01/99	07:05–07:47	1.02	20	Hyades 64	1.06
3903 Kliment Ohridski	Sq	09/29/97	11:47–12:30	1.16	20	93-101	1.13
3944 Halliday	V(SMASS I)	05/02/98	11:11–11:44	1.22	16	102-1081	1.08
3968 Koptelov	V(SMASS I)	04/29/98	08:33–09:11	1.30	20	102-1081	1.07
4005 Dyagilev	J(SMASS I)	02/08/97	10:43–11:31	1.02	20	Hyades 64	1.01
4051 Hatanaka	Sq	01/05/98	10:54–11:45	1.12	20	102-1081	1.20
4062 Schiaparelli	S(SMASS I)	03/01/99	07:55–08:36	1.02	20	Hyades 64	1.06
4142 Dersu-Uzala	A	09/16/98	14:52–15:11	1.04	10	Hyades 64	1.00
4145 Maximova	S(SMASS I)	09/15/98	12:32–13:05	1.05	16	93-101	1.08
4147 Lennon	V(SMASS I)	04/29/98	07:24–08:08	1.14	18	102-1081	1.07
4188 Kitezh	V	09/15/98	14:40–15:00	1.01	6	Hyades 64	1.01
4215 Kamo	V	09/15/98	10:28–11:00	1.03	16	112-1333	1.06
4311 Zguridi	V	05/07/00	10:33–11:01	1.25	14	102-1081	1.07
4407 Taihaku	Sa	05/07/00	11:09–11:36	1.36	14	102-1081	1.07
4512 Sinuhe	Sa	03/01/99	09:48–09:58	1.01	10	Hyades 64	1.06
4606 Saheki	S(SMASS I)	10/01/97	10:48–11:21	1.13	16	93-101	1.06
4713 Steel	A	02/27/99	10:01–10:34	1.12	14	Hyades 64	1.06
4900 Maymelou	V	05/23/99	13:28–14:01	1.24	14	102-1081	1.18
5195 Kaendler	Sl	05/06/00	12:00–12:23	1.28	12	102-1081	1.07
5840 1978 ON	Ld	02/28/99	09:56–10:36	1.01	10	Hyades 64	1.08
7081 Ludibunda	K	05/07/00	12:31–13:03	1.32	16	102-1081	1.07

[a] Dates (month/day/year) and times of the observations are given in universal time (UT).
[b] The quoted airmass is the average airmass for the set of observations.
[c] The number of images gives the number of exposures that were used in the reduction of the asteroid spectrum.
[d] Standard stars that have numbers for names are from the Landolt (1973) listing of ultraviolet, blue, visible standard stars.
[e] Vesta was observed in SMASSII; however, the SMASS I data overlap the SMASSIR data better.
[f] The two sets of 3628 Božněmcová spectra were combined since they were taken a few hours apart.

APPENDIX B

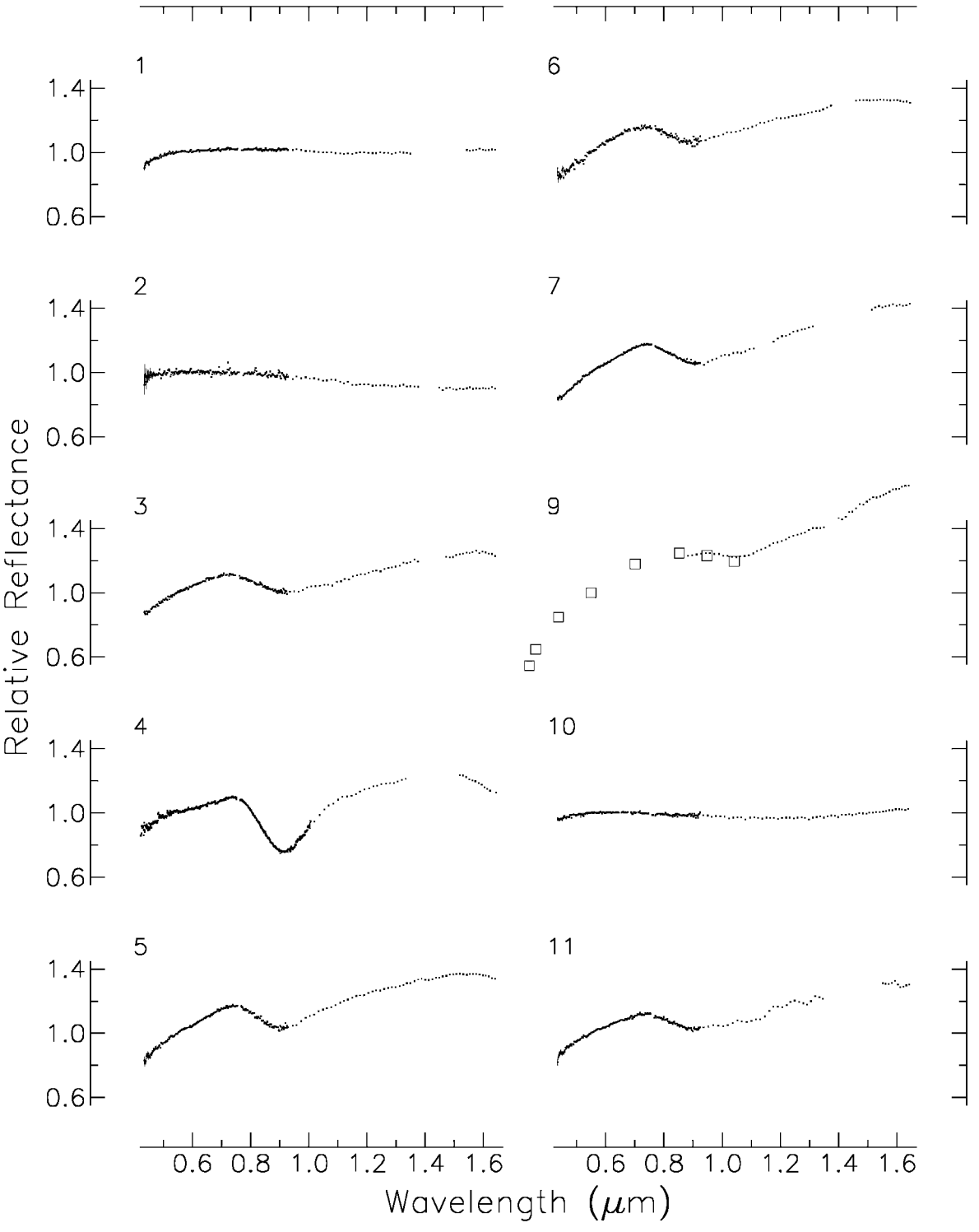
1
2
3
4
5
6
7
9
10
11
1.4
1.0
0.6
Relative Reflectance
0.6 0.8 1.0 1.2 1.4 1.6
Wavelength (μm)

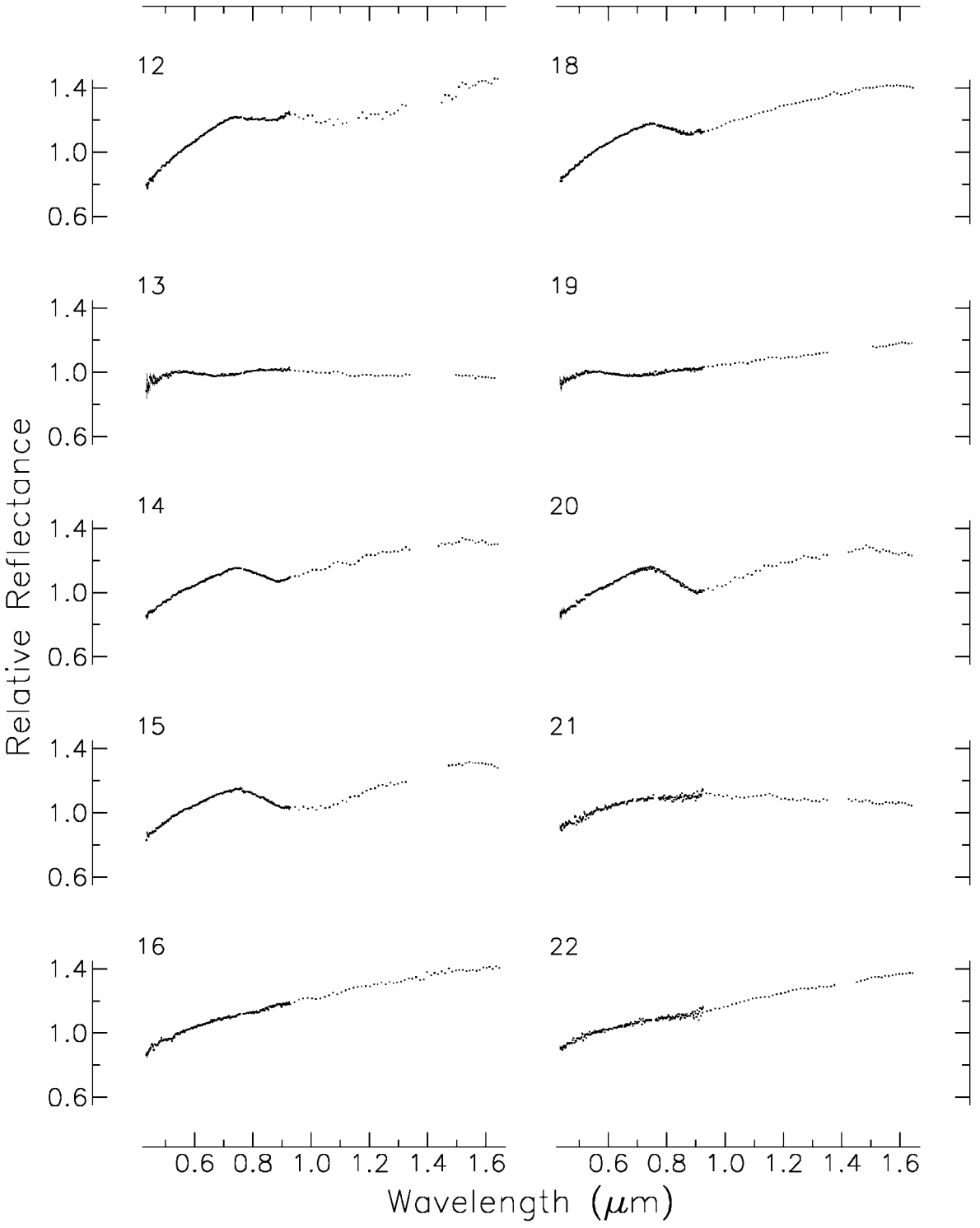
12
18
13
19
14
20
15
21
16
22
1.4
1.0
0.6
Relative Reflectance
0.6 0.8 1.0 1.2 1.4 1.6
Wavelength (μm)

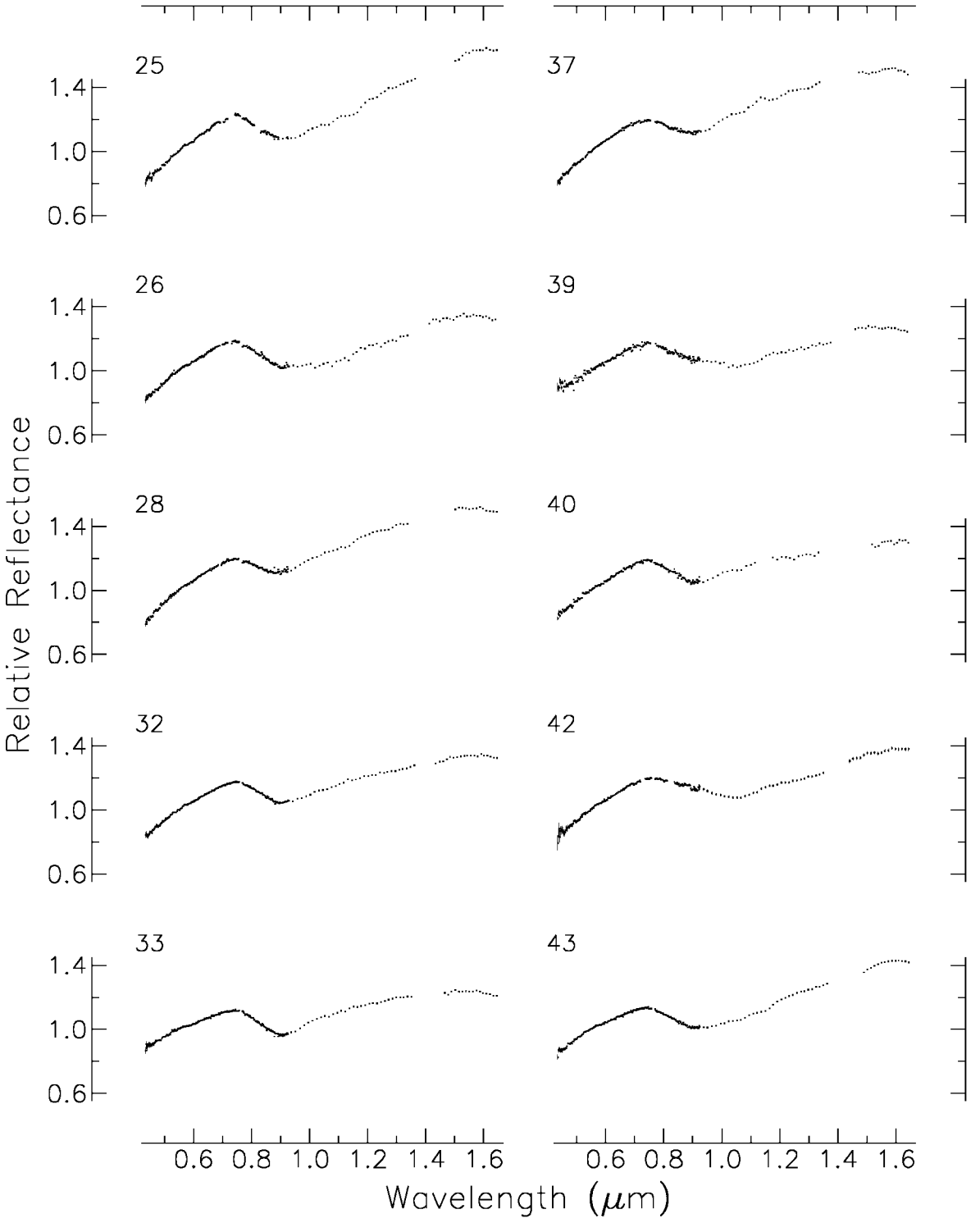
25
37
26
39
28
40
32
42
33
43
1.4
1.0
0.6
Relative Reflectance
0.6 0.8 1.0 1.2 1.4 1.6
Wavelength (μm)

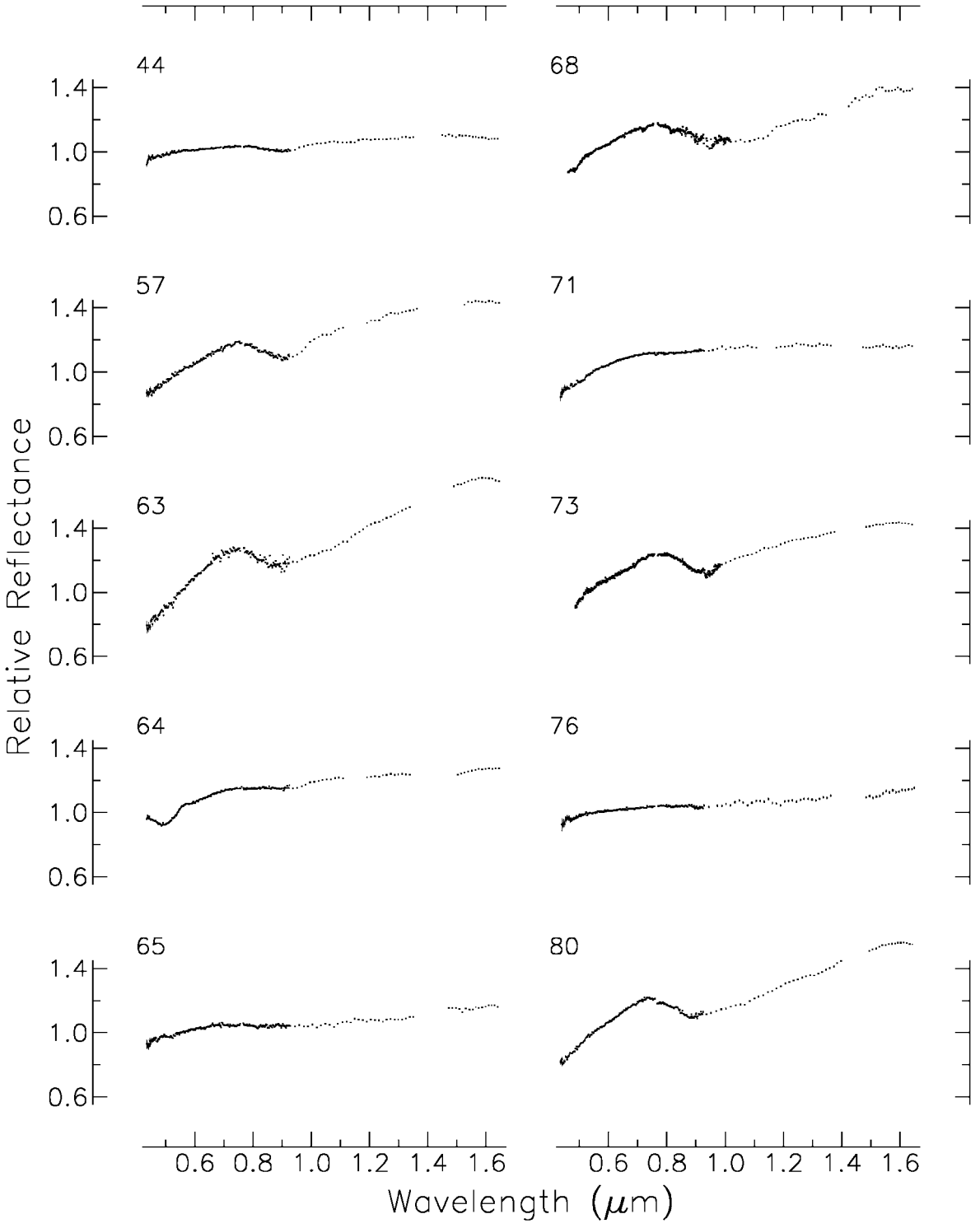
44
68
57
71
63
73
64
76
65
80
1.4
1.0
0.6
Relative Reflectance
0.6 0.8 1.0 1.2 1.4 1.6
Wavelength (μm)

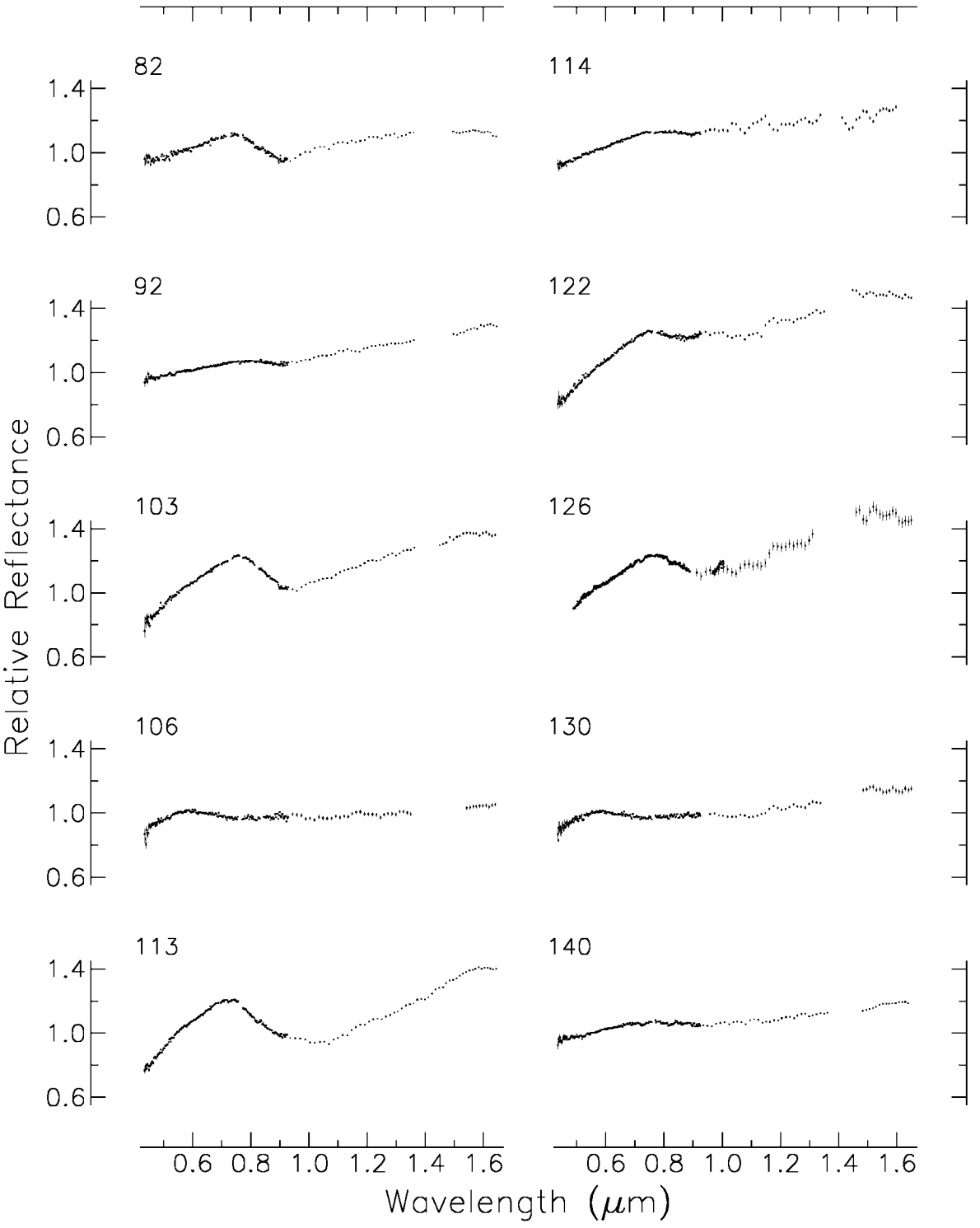
82
114
92
122
103
126
106
130
113
140
1.4
1.0
0.6
Relative Reflectance
0.6 0.8 1.0 1.2 1.4 1.6
Wavelength (μm)

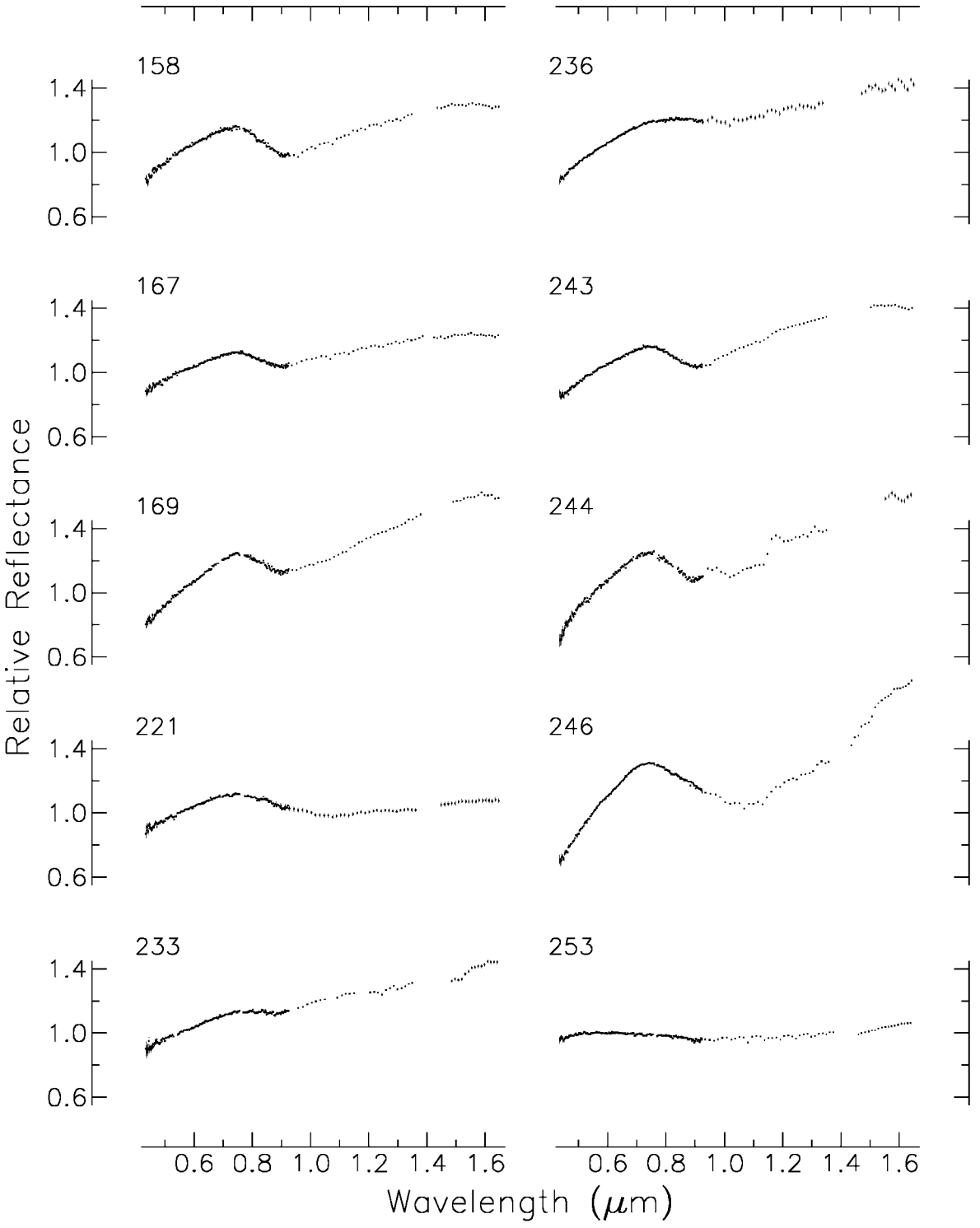
158
236
167
243
169
244
221
246
233
253
1.4
1.0
0.6
Relative Reflectance
0.6 0.8 1.0 1.2 1.4 1.6
Wavelength (μm)

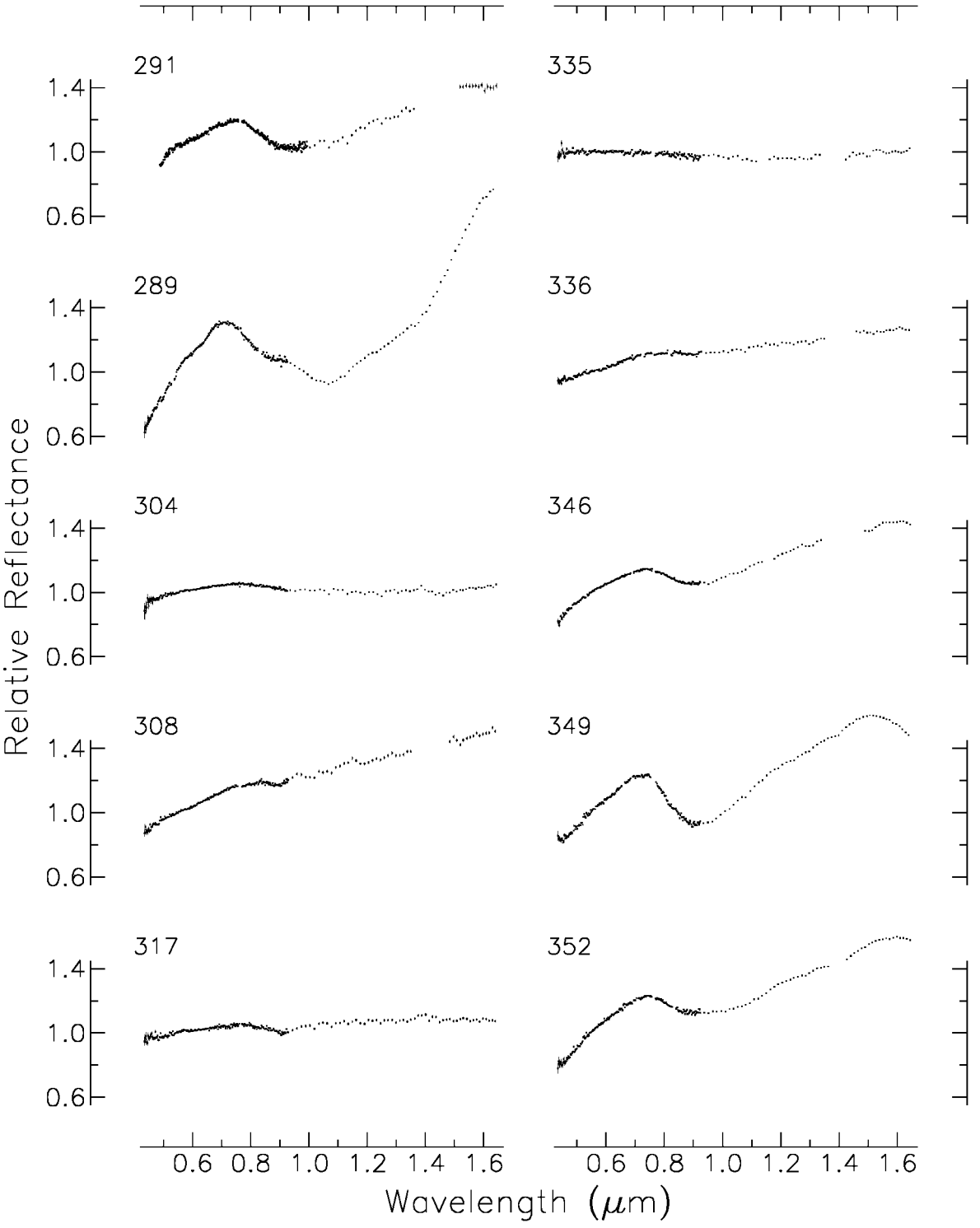
291
335
289
336
304
346
308
349
317
352
1.4
1.0
0.6
Relative Reflectance
0.6 0.8 1.0 1.2 1.4 1.6
Wavelength (μm)

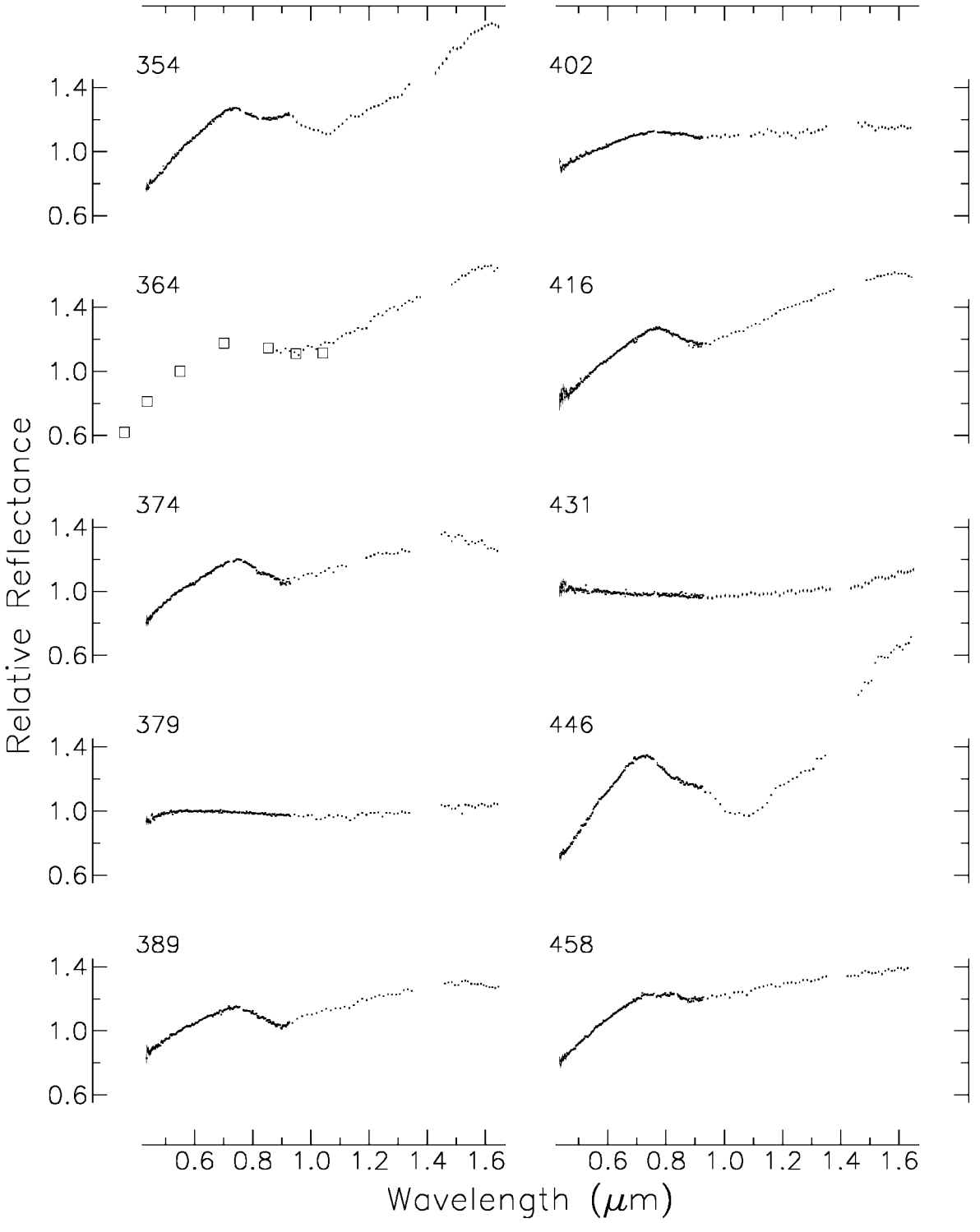
354
402
364
416
374
431
379
446
389
458
1.4
1.0
0.6
Relative Reflectance
0.6 0.8 1.0 1.2 1.4 1.6
Wavelength (μm)

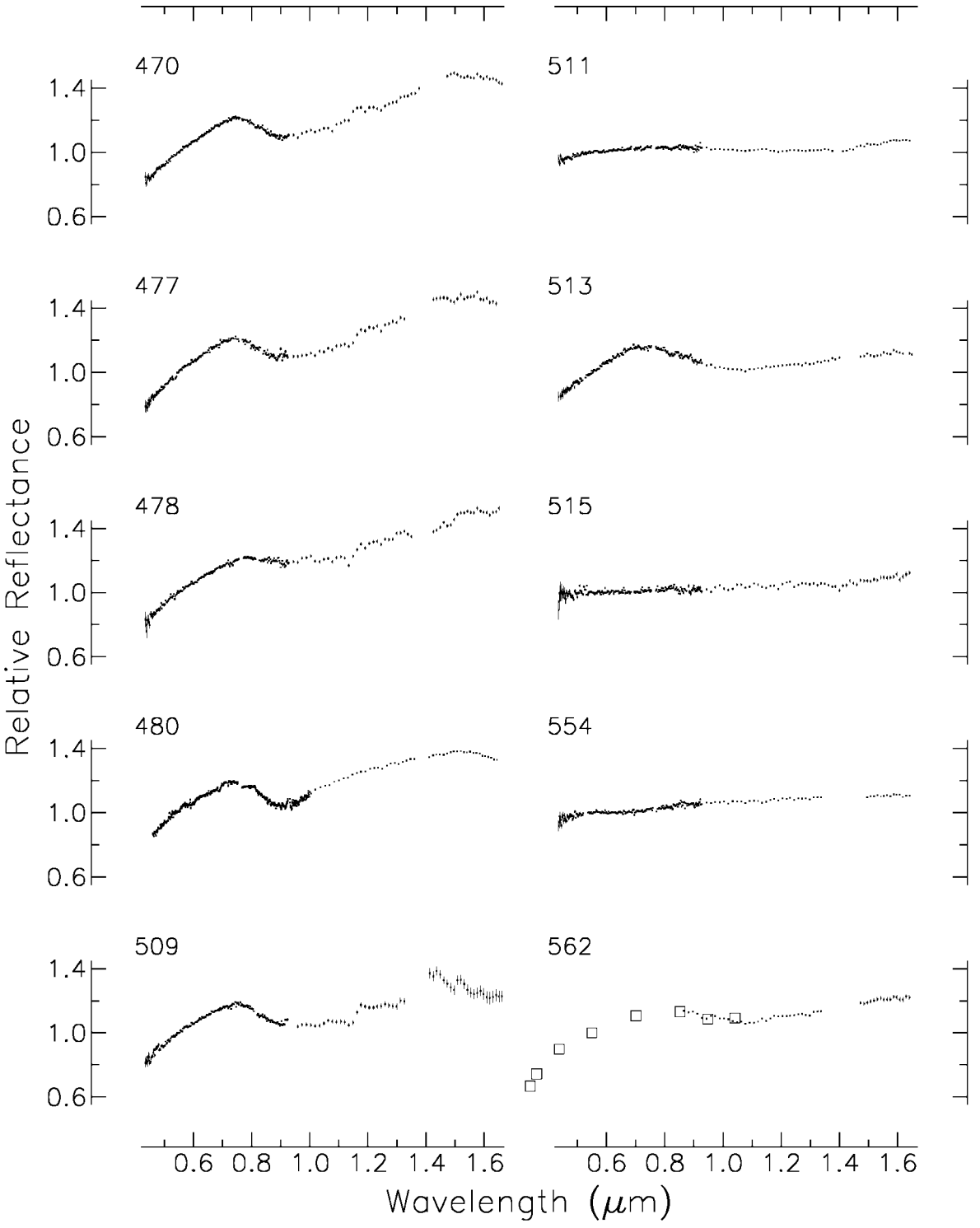
470
511
477
513
478
515
480
554
509
562
1.4
1.0
0.6
Relative Reflectance
0.6 0.8 1.0 1.2 1.4 1.6
Wavelength (μm)

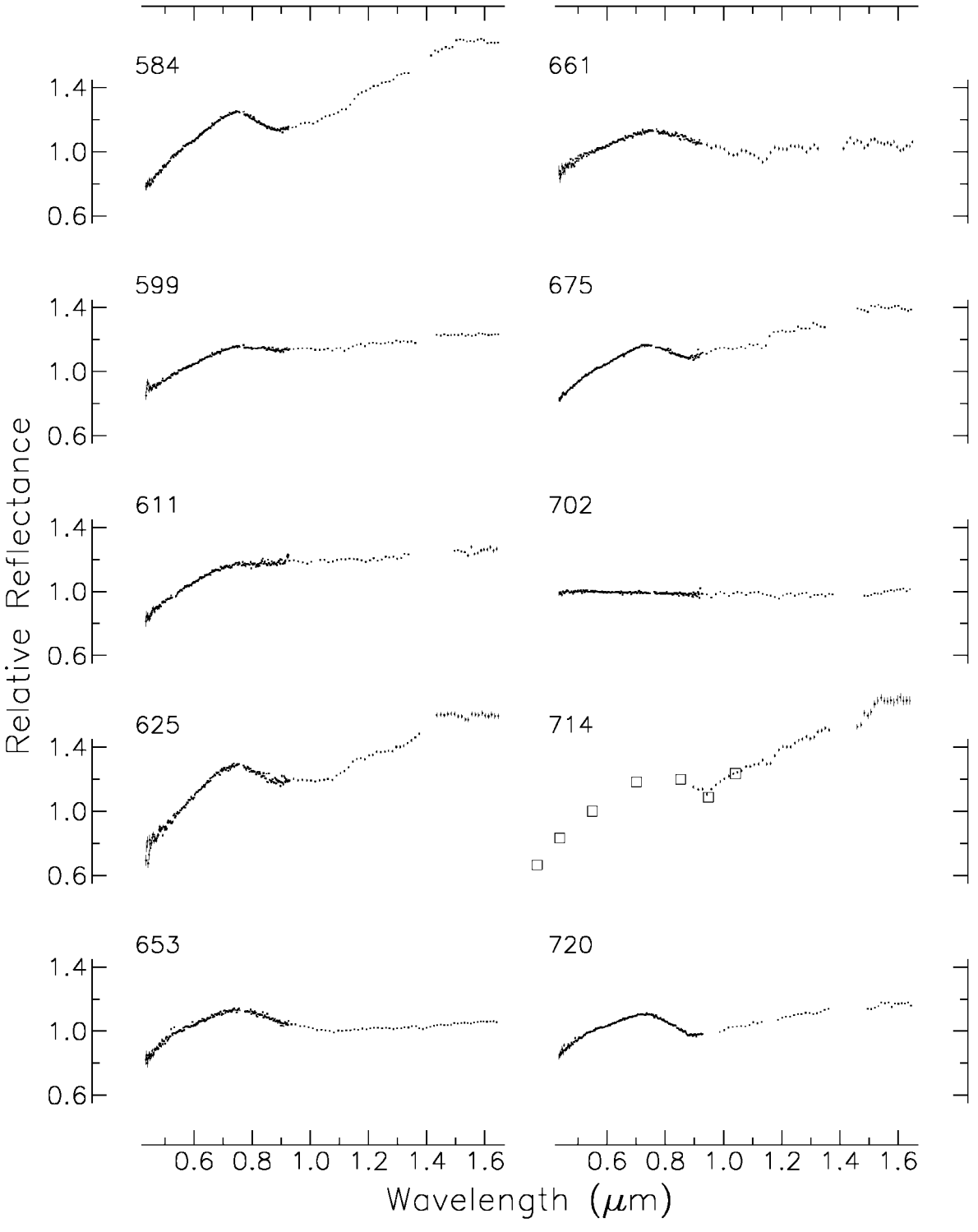
584
661
599
675
611
702
625
714
653
720
1.4
1.0
0.6
Relative Reflectance
0.6 0.8 1.0 1.2 1.4 1.6
Wavelength (μm)

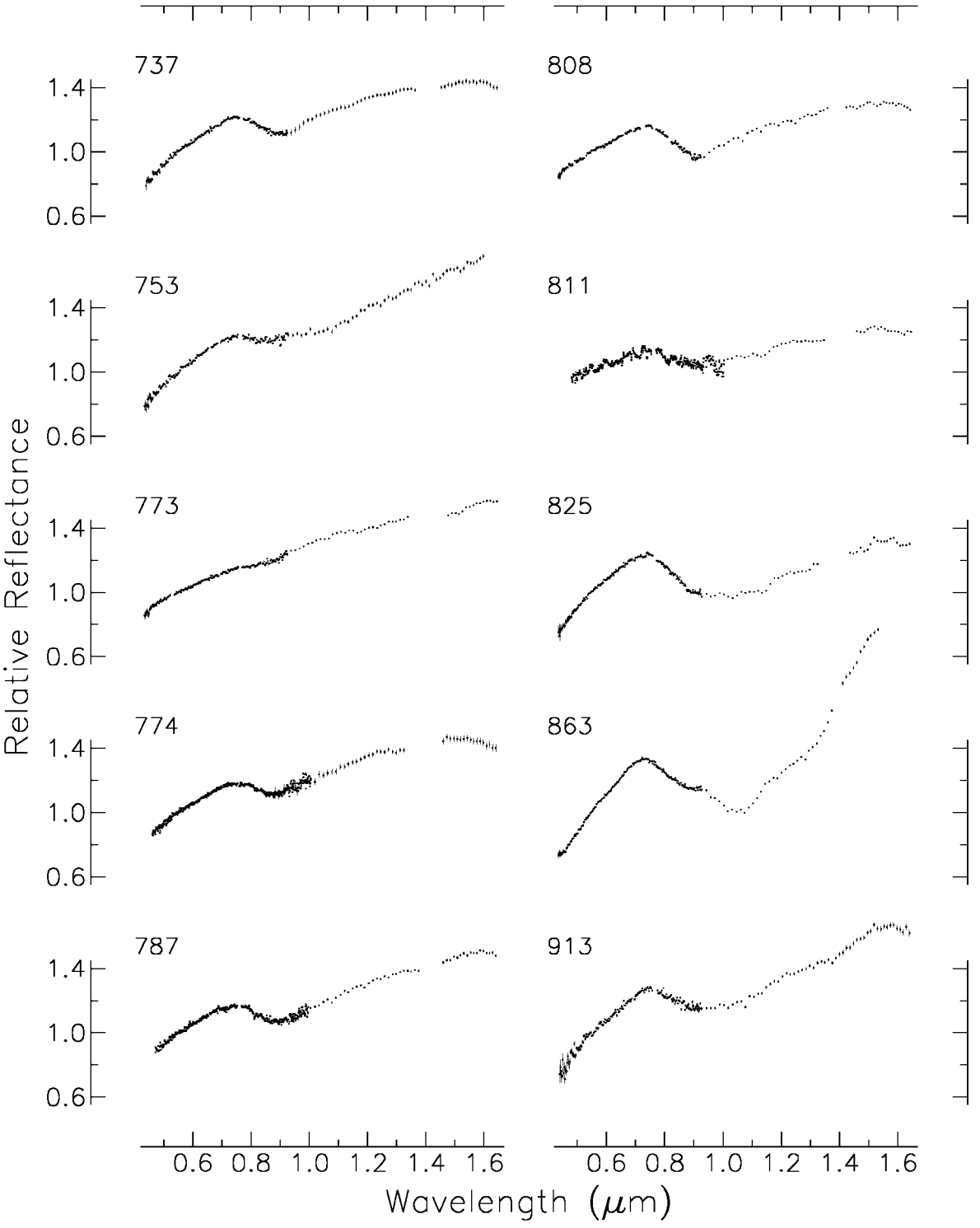
737
808
753
811
773
825
774
863
787
913
1.4
1.0
0.6
Relative Reflectance
0.6 0.8 1.0 1.2 1.4 1.6
Wavelength (μm)

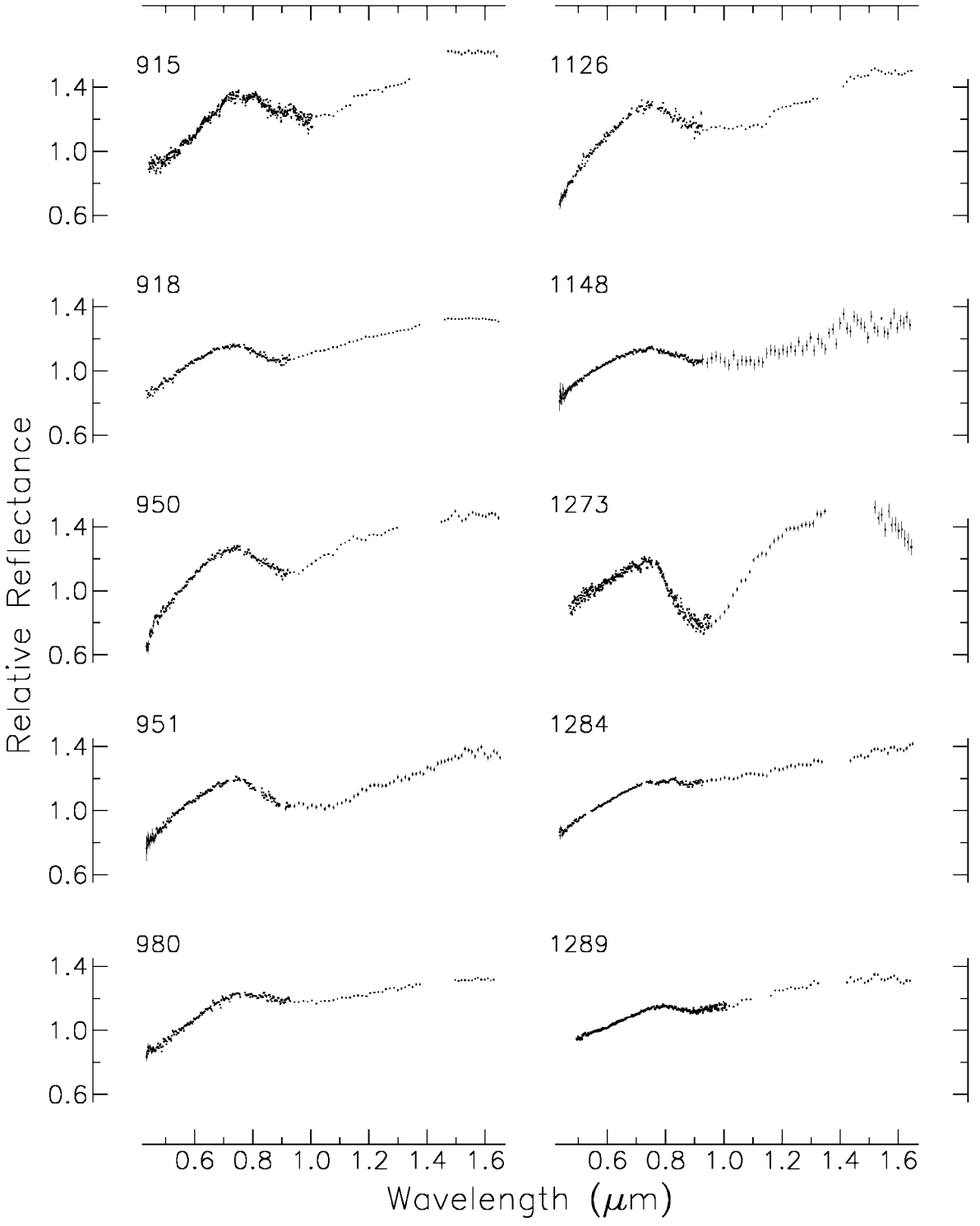
915
1126
918
1148
950
1273
951
1284
980
1289
Relative Reflectance
1.4
1.0
0.6
0.6 0.8 1.0 1.2 1.4 1.6
Wavelength (μm)

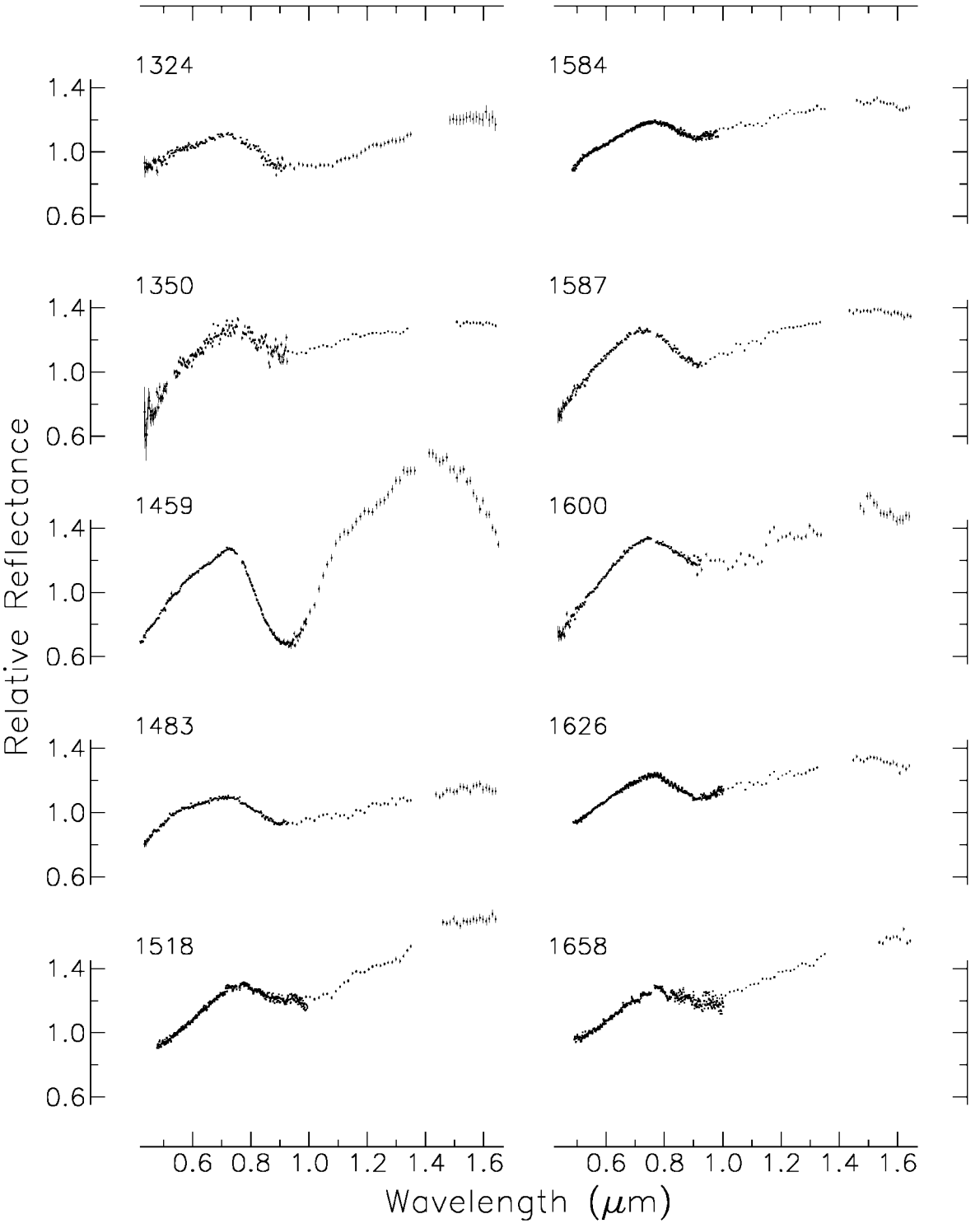
1324
1584
1350
1587
1459
1600
1483
1626
1518
1658
1.4
1.0
0.6
Relative Reflectance
0.6 0.8 1.0 1.2 1.4 1.6
Wavelength (μm)

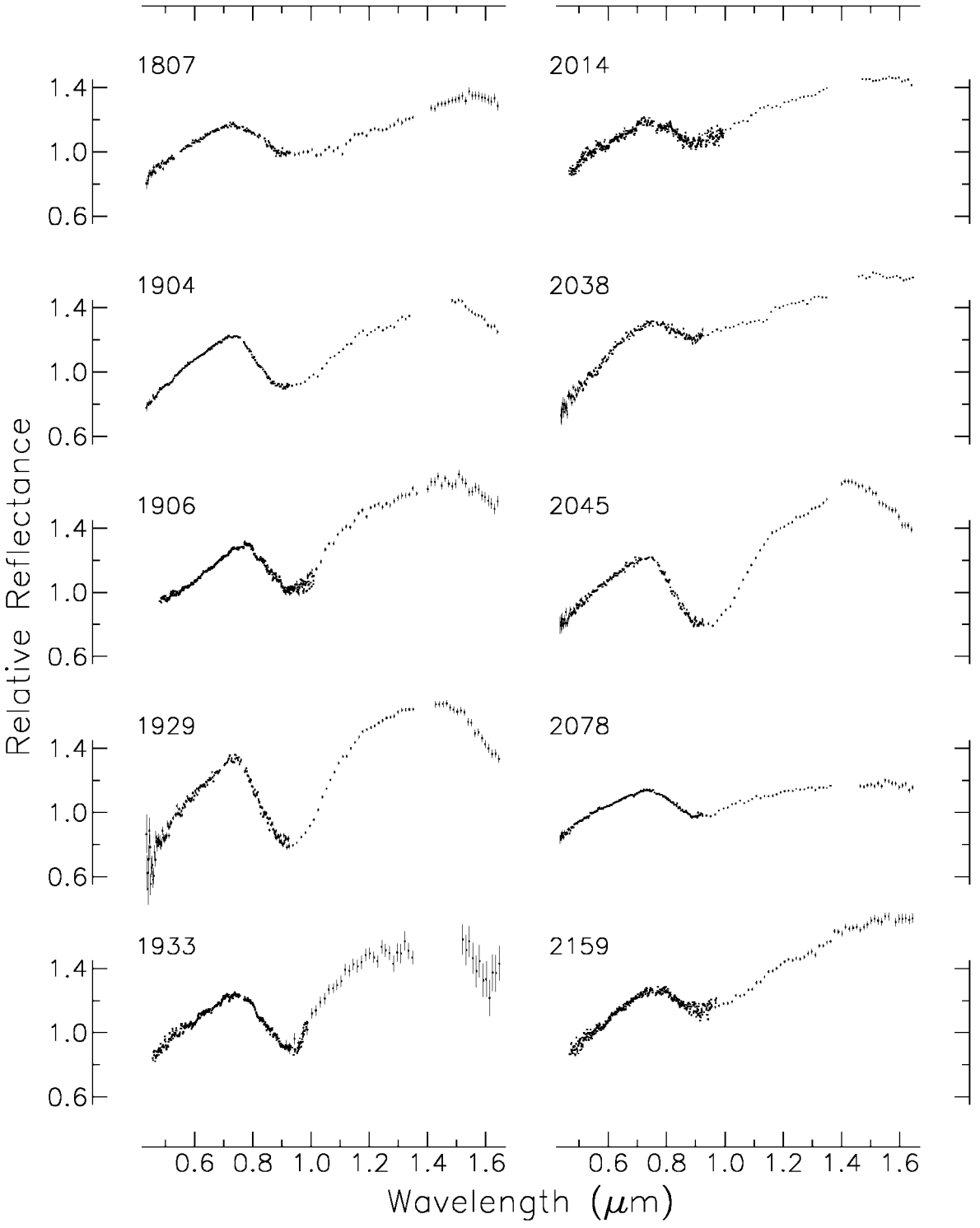
1807
2014
1904
2038
1906
2045
1929
2078
1933
2159
1.4
1.0
0.6
Relative Reflectance
0.6 0.8 1.0 1.2 1.4 1.6
Wavelength (μm)

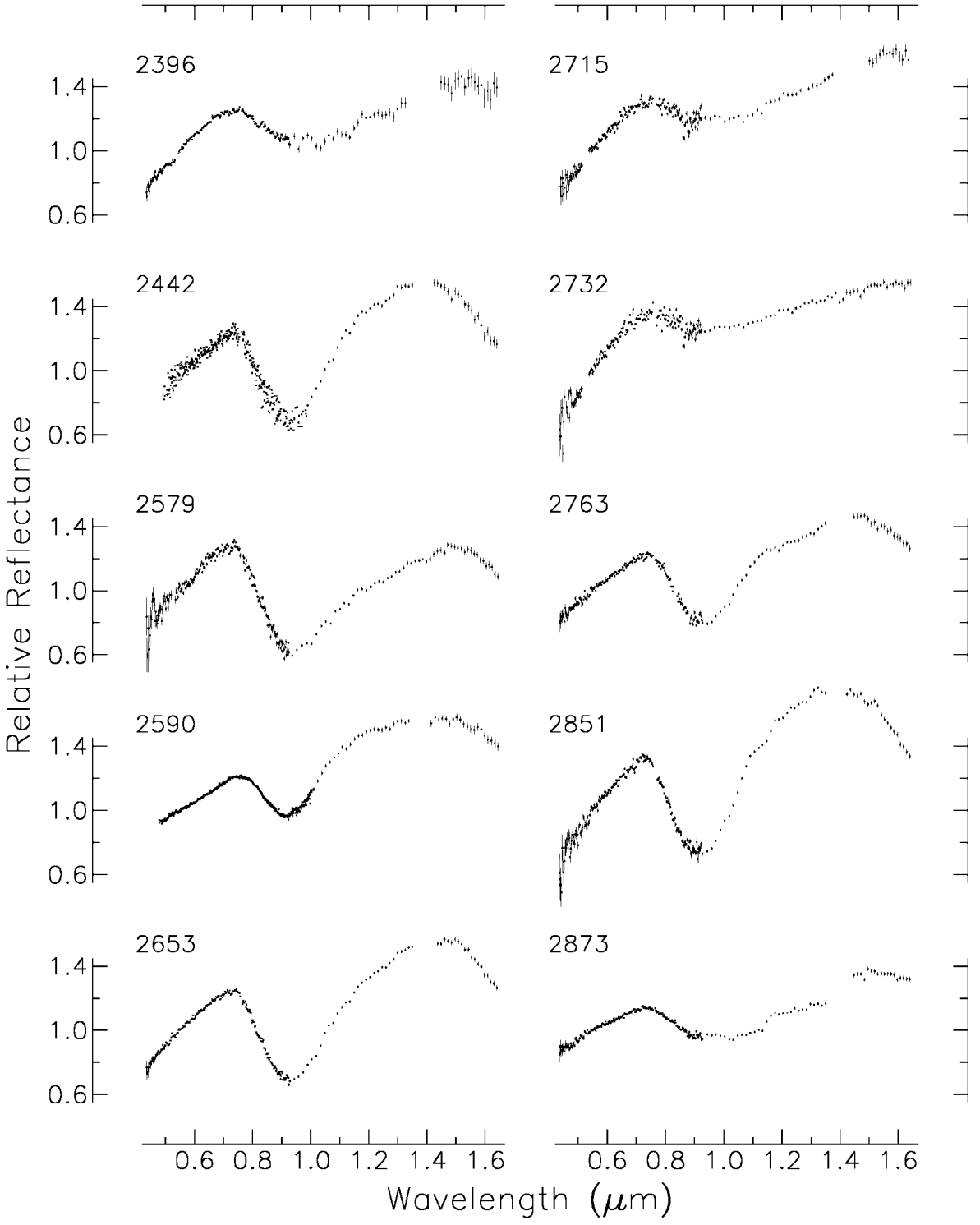
2396
2715
2442
2732
2579
2763
2590
2851
2653
2873
1.4
1.0
0.6
Relative Reflectance
0.6 0.8 1.0 1.2 1.4 1.6
Wavelength (μm)

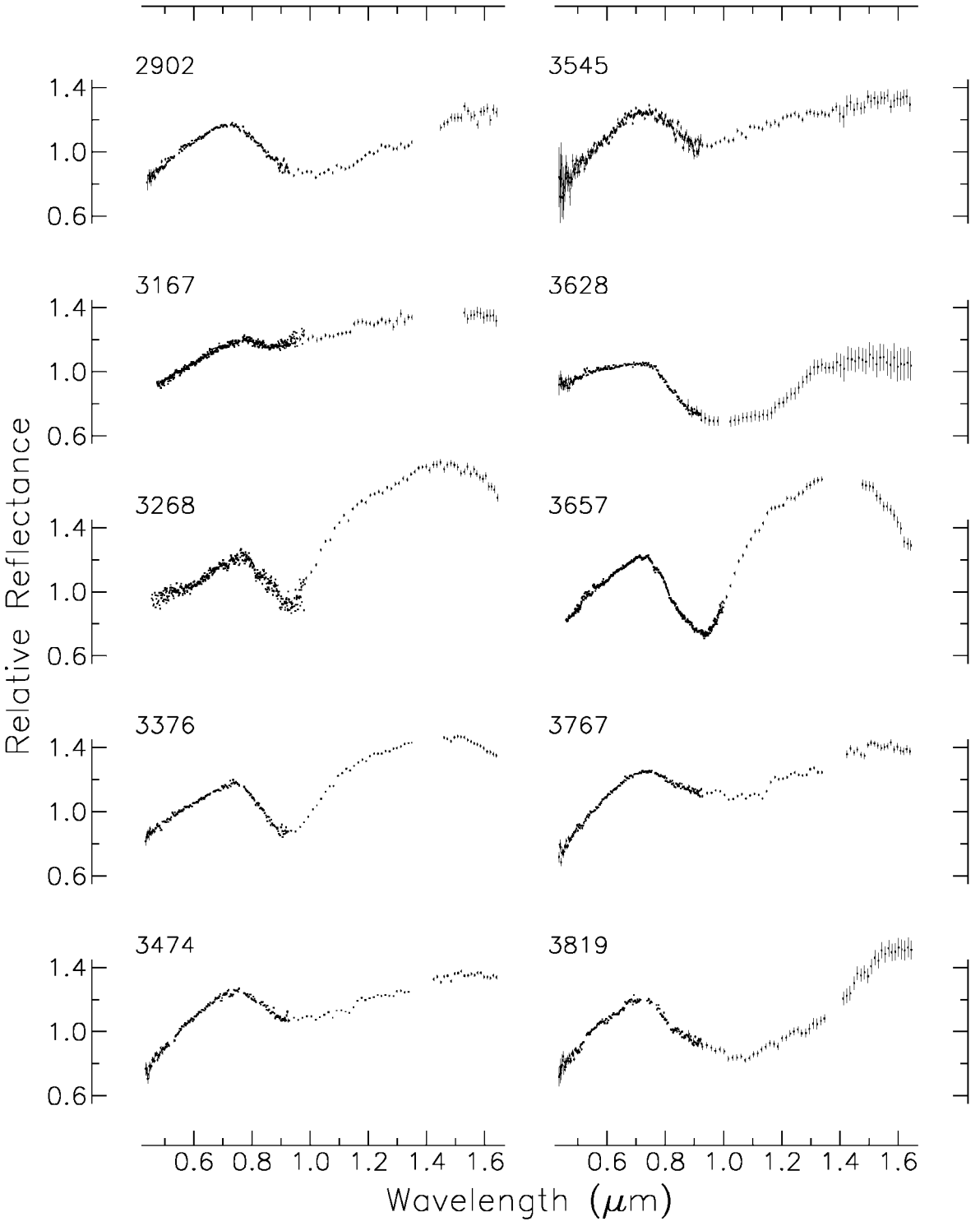
2902
3545
3167
3628
3268
3657
3376
3767
3474
3819
Relative Reflectance
1.4
1.0
0.6
0.6 0.8 1.0 1.2 1.4 1.6
Wavelength (μm)

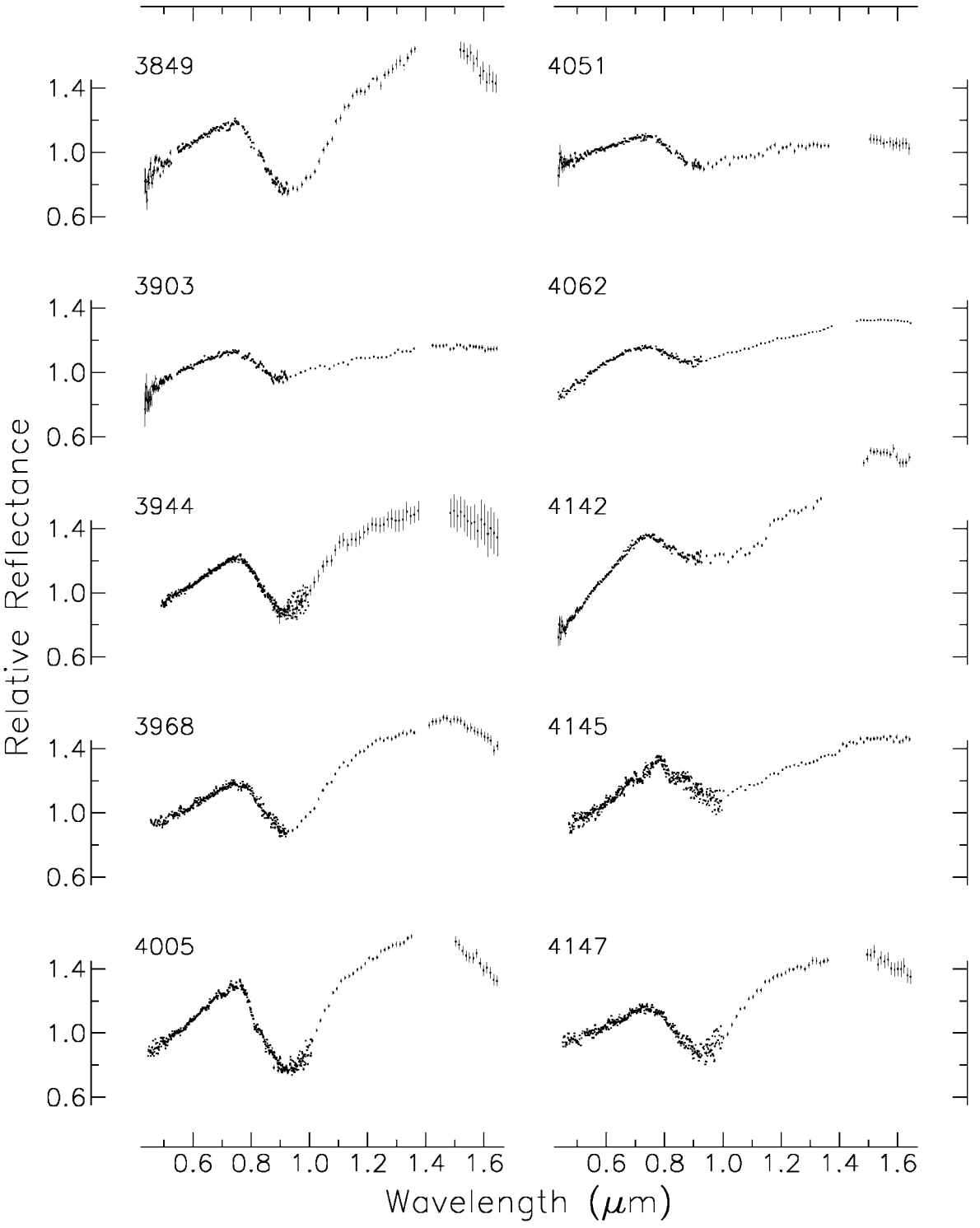
3849
4051
3903
4062
3944
4142
3968
4145
4005
4147
1.4
1.0
0.6
Relative Reflectance
0.6 0.8 1.0 1.2 1.4 1.6
Wavelength (μm)

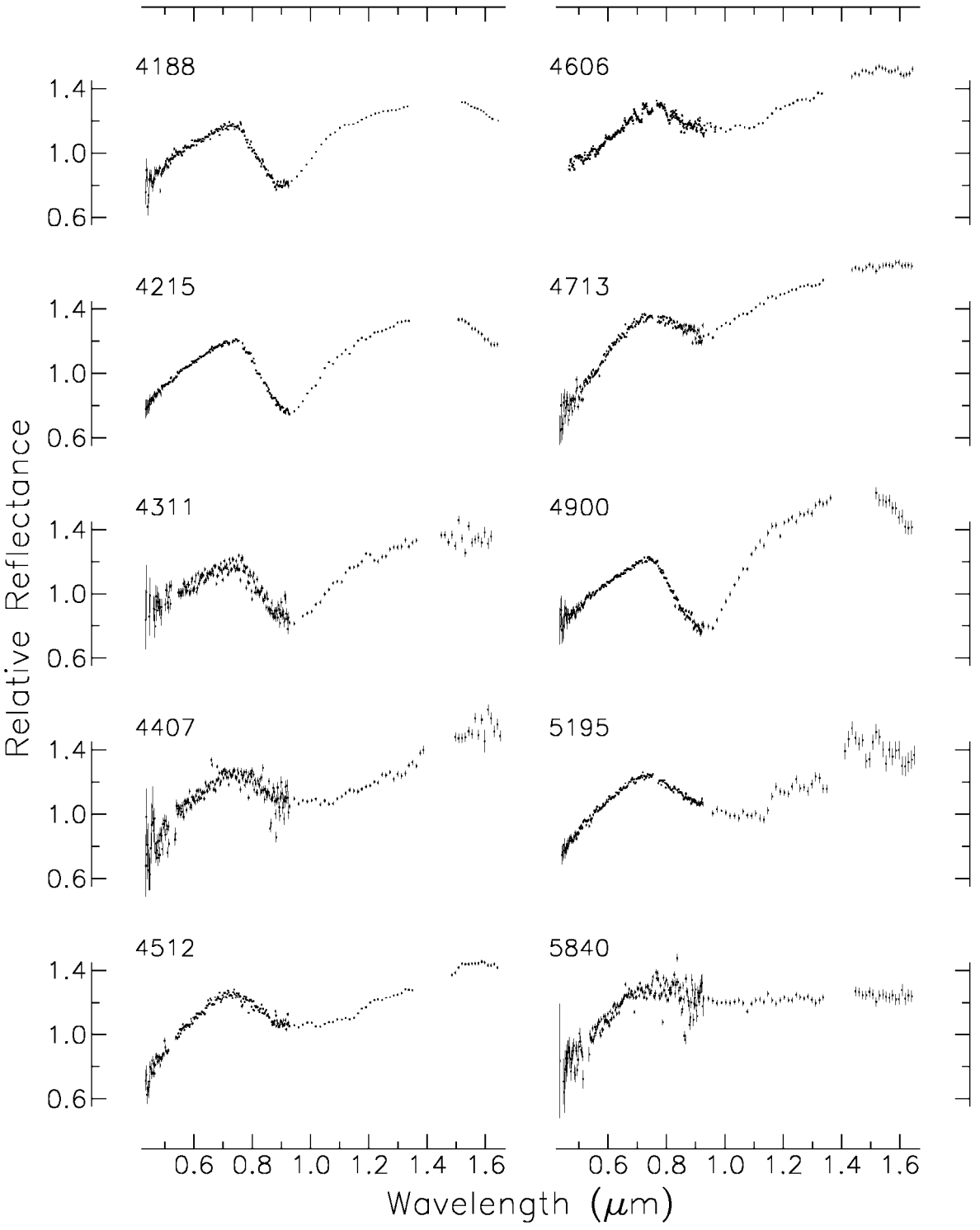
4188
4606
4215
4713
4311
4900
4407
5195
4512
5840
1.4
1.0
0.6
Relative Reflectance
0.6 0.8 1.0 1.2 1.4 1.6
Wavelength (μm)

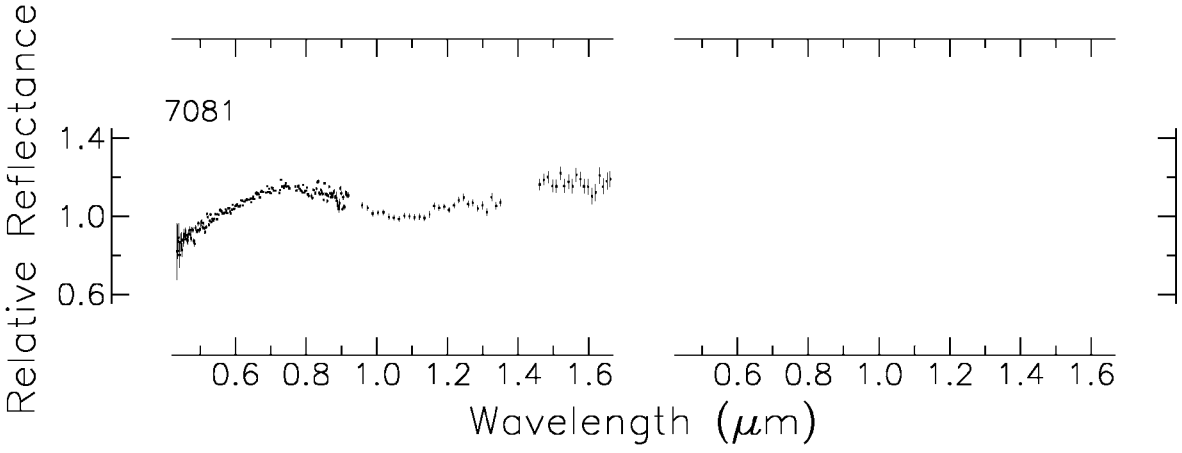

ACKNOWLEDGMENTS

We are highly grateful to April Deet for the IRAF data processing of the final group of SMASSIR measurements, a critical step for the timely and successful completion of the manuscript. This research was primarily supported by NASA Grant NAG5-3939 and NSF Grant AST-9530282 to R.P.B. Measurements of the eucrite EET 87542 (RELAB ID TB-RPB-014) and the diogenite LAP 91900 (TB-RPB-018) were made at Brown University's Keck/NASA Reflectance Experiment Laboratory, which is a multi-user facility supported by NASA Grant NAG5-3871. The authors thank Mike Gaffey and Daniela Lazzaro for their reviews, which greatly improved the manuscript.

REFERENCES

Adams, J. B. 1974. Visible and near-infrared diffuse reflectance spectra of pyroxenes as applied to remote sensing of solid objects in the Solar System. *J. Geophys. Res.* **87**, 4829–4836.

Adams, J. B. 1975. Interpretation of visible and near-infrared diffuse reflectance spectra of pyroxenes and other rock-forming minerals. In *Infrared and Raman Spectroscopy of Lunar and Terrestrial Minerals* (C. Karr III, Ed.), pp. 91–116. Academic Press, New York.

Asphaug, E. 1997. Impact origin of the Vesta family. *Meteor. Planet. Sci.* **32**, 965–980.

Bell, J. F. 1988. A probable asteroidal parent body for the CV or CO chondrites. *Meteoritics* **23**, 256–257 (abstract).

Bell, J. F., P. D. Owensby, B. R. Hawke, and M. J. Gaffey 1988. The 52-color asteroid survey: Final results and interpretation. *Lunar Planet. Sci.* **XIX**, 57–58 (abstract).

Binzel, R. P., and S. Xu 1993. Chips off of Asteroid 4 Vesta: Evidence for the parent body of basaltic achondrite meteorites. *Science* **260**, 186–191.

Binzel, R. P., S. Xu, S. J. Bus, M. F. Skrutskie, M. R. Meyer, P. Knezek, and E. S. Barker 1993. Discovery of a main-belt asteroid resembling ordinary chondrite meteorites. *Science* **262**, 1541–1543.

Binzel, R. P., A. W. Harris, S. J. Bus, and T. H. Burbine 2001a. Spectral properties of near-Earth objects: Palomar and IRTF results for 48 objects including spacecraft targets (9969) Braille and (10302) 1989 ML. *Icarus* **151**, 139–149.

Binzel, R. P., A. S. Rivkin, S. J. Bus, J. M. Sunshine, and T. H. Burbine 2001b. MUSES-C Target Asteroid 1998 SF36: A reddened ordinary chondrite. *Meteor. Planet. Sci.* **36**, 1167–1172.

Brearley, A. J., and R. H. Jones 1998. Chondritic meteorites. In *Reviews in Mineralogy, Planetary Materials* (J. J. Papike, Ed.), Vol. 36, pp. 313–398. Mineralogical Society of America, Washington, DC.

Burbine, T. H., Jr. 2000. *Forging Asteroid–Meteorite Relationships through Reflectance Spectroscopy.* Ph.D. thesis. Massachusetts Institute of Technology, Cambridge.

Burbine, T. H., R. P. Binzel, S. J. Bus, and B. E. Clark 2001a. K asteroids and CO3/CV3 chondrites. *Meteor. Planet. Sci.* **36**, 245–253.

Burbine, T. H., P. C. Buchanan, R. P. Binzel, S. J. Bus, T. Hiroi, J. L. Hinrichs, A. Meibom, and T. J. McCoy 2001b. Vesta, vestoids, and the HEDs: Relationships and the origin of spectral differences. *Meteor. Planet. Sci.* **36**, 761–781.

Bus, S. J. 1999. *Compositional Structure in the Asteroid Belt: Results of a Spectroscopic Survey.* Ph.D. thesis. Massachusetts Institute of Technology, Cambridge.

Bus, S. J., and R. P. Binzel 2002a. Phase I of the small main-belt asteroid spectroscopic survey: The observations. *Icarus* **158**, 106–145.

Bus, S. J., and R. P. Binzel 2002b. Phase II of the small main-belt asteroid spectroscopic survey: A feature-based taxonomy. *Icarus* **158**, 146–177.

Bus, S. J., J. M. Sunshine, R. P. Binzel, and T. H. Burbine 2001. Investigating the spectral continuum between A- and S-type asteroids. *Meteor. Planet. Sci.* **36**, A33 (abstract).

Carvano, J. M., D. Lazzaro, T. Mothé-Diniz, C. A. Angeli, and M. Florczak 2001. Spectroscopic survey of the Hungaria and Phocaea dynamical groups. *Icarus* **149**, 173–189.

Clark, B. E., J. F. Bell, F. P. Fanale, and D. J. O'Connor 1995. Results of seven-color asteroid survey: Infrared spectral observations of ~50-km size S-, K-, and M-type asteroids. *Icarus* **113**, 387–402.

Cloutis, E. A., and M. J. Gaffey 1991. Pyroxene spectroscopy revisited: Spectral-compositional correlations and relationship to geothermometry. *J. Geophys. Res.* **96**, 22,809–22,826.

Cloutis, E. A., M. J. Gaffey, T. L. Jackowski, and K. L. Reed 1986. Calibrations of phase abundance, composition, and particle size distribution for olivine-orthopyroxene mixtures from reflectance spectra. *J. Geophys. Res.* **91**, 11,641–11,653.

Cloutis, E. A., M. J. Gaffey, D. G. W. Smith, and R. St. J. Lambert 1990. Metal silicate mixtures: Spectral properties and applications to asteroid taxonomy. *J. Geophys. Res.* **95**, 8323–8338.

Consolmagno, G. J., and M. J. Drake 1977. Composition and evolution of the eucrite parent body: Evidence from rare Earth elements. *Geochim. Cosmochim. Acta* **41**, 1271–1282.

Cruikshank, D. P., and W. K. Hartmann 1984. The meteorite-asteroid connection: Two olivine-rich asteroids. *Science* **223**, 281–283.

Gaffey, M. J. 1976. Spectral reflectance characteristics of the meteorite classes. *J. Geophys. Res.* **81**, 905–920.

Gaffey, M. J. 1984. Rotational spectral variations of Asteroid (8) Flora: Implications for the nature of the S-type asteroids and for the parent bodies of the ordinary chondrites. *Icarus* **60**, 83–114.

Gaffey, M. J., J. F. Bell, R. H. Brown, T. H. Burbine, J. L. Piatek, K. L. Reed, and D. A. Chaky 1993. Mineralogical variations within the S-type asteroid class. *Icarus* **106**, 573–602.

Hinrichs, J. L., P. G. Lucey, M. S. Robinson, A. Meibom, and A. N. Krot 1999. Implications of temperature-dependent near-IR spectral properties of common minerals and meteorites for remote sensing of asteroids. *Geophys. Res. Lett.* **26**, 1661–1664.

Hiroi, T., J. F. Bell, H. Takeda, and C. M. Pieters 1993. Spectral comparison between olivine-rich asteroids and pallasites. *Proc. NIPR Symp. Antarct. Meteorites* **6**, 234–245.

Hua, X., and P. R. Buseck 1995. Fayalite in the Kaba and Mokoia carbonaceous chondrites. *Geochim. Cosmochim. Acta* **59**, 563–578.

Kelley, M. S., F. Vilas, M. J. Gaffey, K. S. Jarvis, A. L. Cochran, and P. A. Abell 2001a. Confirmation of a genetic link between Asteroids 4 Vesta and 1929 Kollaa: Quantified compositional evidence. *Meteor. Planet. Sci.* **36**, A95 (abstract).

Kelley, M. S., F. Vilas, S. M. Lederer, K. S. Jarvis, S. M. Larson, and P. A. Abell 2001b. Analysis of data obtained during the March 2001 observing campaign of the Muses-C target asteroid 1998 SF36. *Meteor. Planet. Sci.* **36**, A95–A96 (abstract).

King, T. V. V., and W. I. Ridley 1987. Relation of the spectroscopic reflectance of olivine to mineral chemistry and some remote sensing implications. *J. Geophys. Res.* **92**, 11,457–11,469.

Landolt, A. U. 1973. UBV photometric sequences in the celestial equatorial selected areas 92-115. *Astron. J.* **87**, 959–1020.

Larson, H. P., and U. Fink 1975. Infrared spectral observations of Asteroid 4 Vesta. *Icarus* **26**, 420–427.

Lazzaro, D., T. Michtchenko, J. M. Carvano, R. P. Binzel, S. J. Bus, T. H. Burbine, T. Mothé-Diniz, M. Florczak, C. A. Angeli, and A. W. Harris 2000. Discovery of a basaltic asteroid in the outer main-belt. *Science* **288**, 2033–2035.

McCord, T. B., J. B. Adams, and T. V. Johnson 1970. Asteroid Vesta: Spectral reflectivity and compositional implications. *Science* **168**, 1445–1447.

Milani, A., and Z. Knežević 1994. Asteroid proper elements and the dynamical structure of the asteroid belt. *Icarus* **107**, 219–254.

Mittlefehldt, D. W., and M. M. Lindstrom 1993. Geochemistry and petrology of a suite of ten Yamato HED meteorites. *Proc. NIPR Symp. Antarct. Meteorites* **6**, 268–292.

Mittlefehldt, D. W., T. J. McCoy, C. A. Goodrich, and A. Kracher 1998. Nonchondritic meteorites from asteroidal bodies. In *Reviews in Mineralogy, Planetary Materials* (J. J. Papike, Ed.), Vol. 36, pp. 4-1–4-195. Mineralogical Society of America, Washington, DC.

Moroz, L. V., A. V. Fisenko, L. F. Semjonova, C. M. Pieters, and N. N. Korotaeva 1996. Optical effects of regolith processes on S-asteroids as simulated by laser shots on ordinary chondrite and other mafic materials. *Icarus* **122**, 366–382.

Reinsch, C. H. 1967. Smoothing by spline functions. *Numer. Math.* **10**, 177–183.

Sasaki, S., K. Nakamura, Y. Hamabe, E. Kurahasi, and T. Hiroi 2001. Production of iron nanoparticles by laser irradiation in a simulation of lunar-like space weathering. *Nature* **419**, 555–557.

Scott, E. R. D., and R. H. Jones 1990. Disentangling nebular and asteroidal features of CO3 carbonaceous chondrite meteorites. *Geochim. Cosmochim. Acta* **54**, 2485–2502.

Sunshine, J. M., and C. M. Pieters 1998. Determining the composition of olivine from reflectance spectroscopy. *J. Geophys. Res.* **103**, 13,675–13,688.

Tholen, D. J. 1984. *Asteroid Taxonomy from Cluster Analysis of Photometry.* Ph.D. thesis. Univ. Arizona, Tucson.

Wahl, W. 1950. The statement of chemical analyses of stony meteorites and the interpretation of the analyses in terms of minerals. *Mineral. Mag.* **29**, 416–426.

Xu, S., R. P. Binzel, T. H. Burbine, and S. J. Bus 1995. Small main-belt asteroid spectroscopic survey: Initial results. *Icarus* **115**, 1–35.

Yamada, M., S. Sasaki, H. Nagahara, A. Fujiwara, S. Hasegawa, H. Yano, T. Hiroi, H. Ohashi, and H. Otake 1999. Simulation of space weathering of planet-forming materials: Nanosecond pulse laser irradiation and proton implantation on olivine and pyroxene samples. *Earth, Planet. Space* **51**, 1255–1265.

Yamaguchi, A., R. N. Clayton, T. K. Mayeda, M. Ebihara, Y. Oura, Y. N. Miura, H. Haramura, K. Misawa, H. Kojima, R. N. Clayton, T. K. Mayeda, and K. Nagao 2002. A new source of basaltic meteorites inferred from Northwest Africa 011. *Science* **296**, 334–336.

Zappalà, V., Ph. Bendjoya, A. Cellino, P. Farinella, and C. Froeschlé 1995. Asteroid families: Search of a 12,487-asteroid sample using two different clustering techniques. *Icarus* **116**, 291–314.

Zellner, B., D. J. Tholen, and E. F. Tedesco 1985. The eight-color asteroid survey: Results for 589 minor planets. *Icarus* **61**, 355–416.